



CZECH TECHNICAL UNIVERSITY IN PRAGUE
FACULTY OF BIOMEDICAL ENGINEERING

Department of Biomedical Technology

**Optimization Of 3D-Bioprinting On Nanofiber Substrates
For Tissue Replacement**

Master thesis

Study programme: Biomedical and Clinical Technology

Study branch: Biomedical Engineering

Author of the master thesis: Kumar Dhruv Ramkrishnan

Supervisor of the master thesis: Ing. Roman Matejka Ph.D.

Kladno, August 2021

I. PERSONAL AND STUDY DETAILS

Student's name: **Ramakrishnan Kumar Dhruv** Personal ID number: **491328**
Faculty: **Faculty of Biomedical Engineering**
Department: **Department of Biomedical Technology**
Study program: **Biomedical and Clinical Technology**
Branch of study: **Biomedical Engineering**

II. MASTER'S THESIS DETAILS

Master's thesis title in English:

Optimization of 3D bioprinting on nanofiber substrates for tissue replacements

Master's thesis title in Czech:

Optimization of 3D bioprinting on nanofiber substrates for tissue replacements

Guidelines:

Design mounting fixtures for planar nanofiber substrates (PCL or collagen based) in 3D bioprinter. Solution must be optimized for work in sterile conditions in a laminar box. Verify these fixtures to withstand sterilization process using autoclave. Optimize 3D printer toolpath generation for using fixtures with attached nanofibers. Verify design with cell experiments involving human or animal primary cells printed in porcine based collagen on nanofibers. Analyze cell proliferation in prepared constructs.

Bibliography / sources:

[1] Lanza, R., Langer, R., Vacanti, J., Principles of Tissue Engineering, ed. 3rd, Elsevier Academic Press, 2007, ISBN 978-0123706157

Name of master's thesis supervisor:

Ing. Roman Matějka

Name of master's thesis consultant:

Date of master's thesis assignment: **15.02.2021**

Assignment valid until: **23.09.2020**

Doc. Ing.
Martin
Rožánek,
Ph.D. Digitálně podepsal
Doc. Ing. Martin
Rožánek, Ph.D.
Datum: 2021.03.04
11:11:14 +01'00'

doc. Ing. Martin Rožánek, Ph.D.
Head of department's signature

prof. MUDr.
Jozef Rosina,
Ph.D., MBA Digitálně podepsal
prof. MUDr. Jozef
Rosina, Ph.D., MBA
Datum: 2021.03.04
13:10:17 +01'00'

prof. MUDr. Jozef Rosina, Ph.D., MBA
Dean's signature

III. ASSIGNMENT RECEIPT

The student acknowledges that the master's thesis is an individual work. The student must produce his/her thesis without the assistance of others, with the exception of provided consultations. Within the master's thesis, the author must state the names of consultants and include a list of references.

.....
Date of assignment receipt

.....
Student's signature

DECLARATION

I hereby declare that I have completed this thesis with the topic “**Optimization of 3D-bioprinting on nanofiber substrates for tissue replacement**” independently and that I have attached an exhaustive list of citations of the employed sources.

I do not have a compelling reason against the use of the thesis within the meaning of Section 60 of Act No. 121/2000 Sb., on copyright, rights related to copyright, and amending some laws (Copyright Act).

B.E. Kumar Dhruv Ramakrishan

ACKNOWLEDGEMENTS

This thesis has been inspired by the outstanding and path-breaking support and thoughts of my research supervisor, Ing. Roman Matějka Ph.D., whose dedication, incisive encouragement, and vision have been instrumental in guiding my efforts. Sir, I can never thank you enough for your continuous support, inspiration, and deep knowledge that have been catalytic in my work. Your work ethic, high standards, and exemplary presence will always remain the guiding force for all those who have been fortunate to have you in their lives. I promise to always strive to live up to the high standards and principles that you stand for. Thank you so much, Sir.

This thesis is also a manifestation of the continued stellar and wonderfully knowledgeable support of the thesis committee members and my colleagues at the Faculty of Biomedical Engineering at the Czech Technical University. I consider myself singularly blessed to have had this opportunity to be part of this amazing team of exceptional professionals and to have been able to utilize the state-of-the-art facilities of this truly world-class institution.

I would also like to thank my family for their support in this endeavor of mine.

This work was supported by the Ministry of Health of the Czech Republic (grant No. NV19-02-00068), and by the Ministry of Education, Youth and Sports of the Czech Republic and European Union funds in Operational Programme Research, Development, and Education, project no. CZ.02.2.69/0.0/0.0/16_018/0002242 and CZ.02.1.01/0.0/0.0/16_017/0002244.



EUROPEAN UNION
European Structural and Investment Funds
Operational Programme Research,
Development and Education



Master's Thesis title

Optimization of 3D Bioprinting on nanofiber substrates for tissue replacements

Abstract

The primary objective of this project was to optimize the bioprinting on nanofiber substrates. We developed the configurations required to print constructs on a square nanofiber sheet of collagen/PCL blend. A fixture was designed specifically for this purpose. The structure was tested in sterile conditions and verified to survive the high temperatures of an autoclave and a custom bioprinter. We programmed the path of the extruding nozzle to function with the nanofiber fixture as the customized bed profile and configurations. The bioink composition had to be optimized along with the printability of the constructs. Cell experimentation was done to check the viability and distribution of cells in the constructs made from bioink. We created an algorithm for image processing and image analysis for cell counting. The printability of the constructs on nanofiber sheets and the analytical data generated via image processing code was then studied to be improved.

Keywords

Bioprinting, Collagen, extrusion printing, PCL, Bioink.

Table of Contents

List of symbols and abbreviations	8
1 Introduction	9
1. Overview of the current state	12
a. Inkjet Bioprinting	13
b. Laser-assisted bioprinting	14
c. Stereolithography	16
d. Extrusion bioprinting	17
e. Hydrogels and Bioink	19
2. Aims of the thesis	23
2 Methods	24
1. Development and fabrication of the fixture	24
a. Fixture design 1 version 1 (B1V1)	25
b. Fixture design 2 version 1 (B2V1)	26
2. Preparation of Printing constructs and optimization of the tool path	27
a. Creating configurations for custom bioprinter	29
3. Verification of design and configurations	38
4. Python script prepared to generate G-code	40
5. Printing on nanofiber substrate	46
6. Image analysis and cell counting	47
3 Results	51
1. Verification of design and configurations	51
2. G-code generated by Python script	53
3. Image analysis and cell counting	55
4 Discussion	58
1. Verification of design and configurations	58
2. G-code generated by python script	58
3. Image analysis and cell counting	59
5 Conclusions	64
List of Literature	65
List of appendices	73

List Of Symbols And Abbreviations

- 1 TE - Tissue Engineering
- 2 FDM - Fused deposition modeling
- 3 LDW - Laser-based direct writing
- 4 LIFT - Laser-induced forward transfer
- 5 CAD - Computer-aided/assisted design
- 6 PVA - Poly(Vinyl Alcohol)
- 7 CPCs - Cartilage Progenitor cells
- 8 SMCs - Smooth muscle cells
- 9 PCL - Polycaprolactone
- 10 MSC - Mesenchymal Stem Cells
- 11 ESC - Embryonic Stem Cells
- 12 iPSCs - Induced Pluripotent Stem Cells
- 13 pASCs - Adipose tissue-derived Porcine Stem Cells
- 14 LoG - Laplacian of Gaussian
- 15 DAPI - 4',6-diamidino-2-phenylindole

1. Introduction

Ever since man began studying himself, his anatomy, and his world, scientists, thinkers, and visionaries have sought to create or replicate nearly anything and everything. Over time, as science and technology evolved and gradually caught up with the seemingly outlandish, far-fetched, and sometimes even impossible quests of human thought, technology and human vision slowly began to converge. It seems that the holy grail of human engineering may now be turning fiction into reality.

Bioprinting three-dimensional constructs for regenerative medicine has become one of the front runners in emerging technologies.[1] Layer by layer deposition of polymeric material with the help of computer-aided slicing technologies has allowed us to create complex, robust, and repeatable structures for large-scale use[2]. The earliest research using polymers to create 3D designs was in 1960 at Battelle Memorial Institute in Ohio[3]. In 1984 Charles Hull came up with the first commercial 3D printer, and soon after, in 1986, he patented his invention for stereolithography. This technology utilized Ultraviolet radiation to solidify a photosensitive polymer layer by layer through a selective mask to give its structure the desired complexities [4].

It was only in the year 1954 that the first-ever successful organ transplant was carried out, and this was done between two identical twins. This was a scientific milestone as it allowed us to break through the immunological barrier and let the recipient accept the donated kidney[5]. Joseph Murray and his team, in 1958, attempted to transplant kidneys in 12 patients. They were disappointed with the results as 11 out of the 12 patients died within a month.

In Paris, from 1960 -1962, Jean Hamburger and Rene' Ku'ss performed four surgeries where kidney transplantation was successfully performed with total body irradiation. These surgeries became the benchmark justification for continued kidney transplantations[6].

While many human dreams, visions, and aspirations depended on simple technologies that emerged with time, the field of three-dimensional bioprinting has opened up new areas of

research such as personalized pharmaceuticals, artificial meat products, and of course bioprinting tissue and organs for regenerative medicine[7]. Engineering tissue like the myocardium, trachea and even Liver tissue are some of the more extensively studied areas of research. Damage to heart muscle during myocardial infarction is fatal and requires the damaged section to be excised and replaced[8].

Professor Anthony Atla, in the year 2006, successfully implanted an ex vivo 3D printed bladder into his patient. More than 14 years of being implanted in the body, this artificial organ is still implanted and perfectly functional[9]. Having successfully transplanting a bladder, Anthony Atla is now attempting to do the same with Kidneys. Artificial kidneys have been developed (For Example, iRAD- implantable Renal Assist Device, which is a self-regulating Bioartificial Kidney the size of a teacup) and show great promise in the treatment of End-Stage Renal Disease (ESRD) [10].

The designing and manufacturing of a 3D printed scaffold require careful consideration of the native tissue. These may be entire organs or specialized tissue like muscle tissue or dermal tissue. The structure of the tissue, along with the concentration of the cells, needs to be constructed in a way that resembles the native tissue. Biomimicry is an important quality for a scaffold to have; physical attributes like the micro-architecture, long-term stability, biodegradability, and vasculature are essential in the development of a functional scaffold[11].

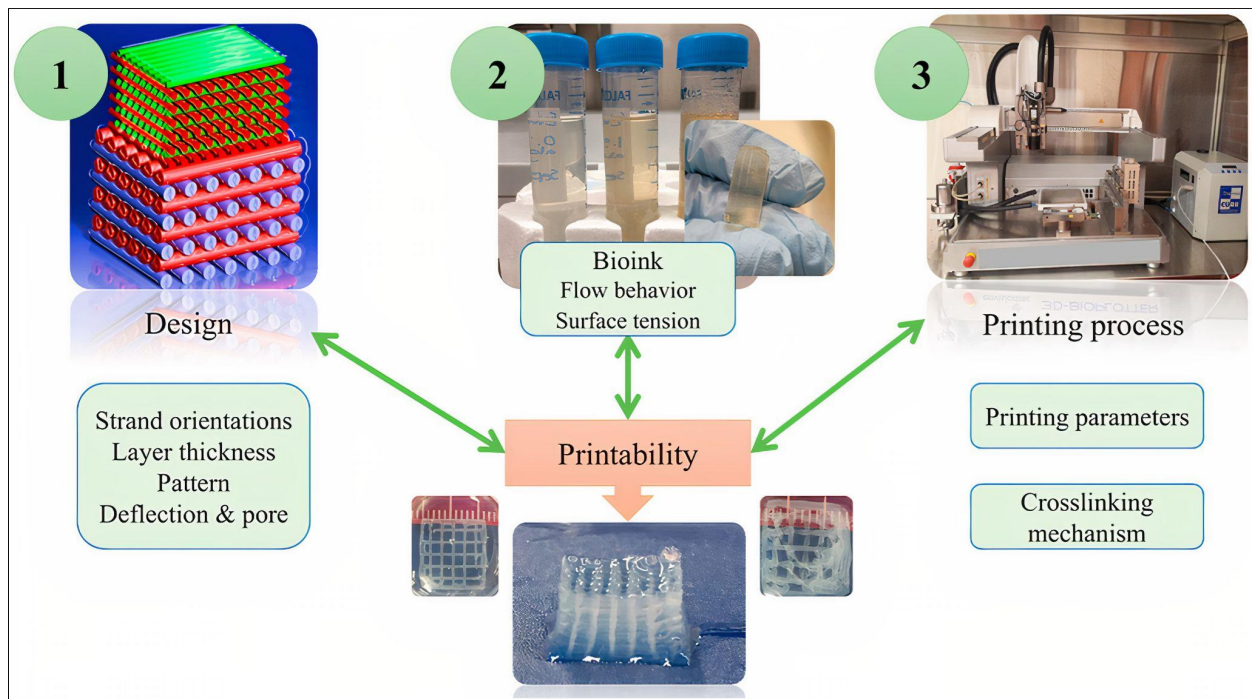


Figure.1.1. Factors affecting printability (Figure adapted from [12])

Broadly speaking, the printability of any construct sits on the shoulders of the three points, as shown in Fig.1.1. The printing construct design is made to be stable, functional, and able to house cells for differentiation. Bioink is a mixture of polymer, growth hormones, nutrients, and stem cells embedded all over the printed construct. Bio inks are based on natural polymers, synthetic polymers, and mixed combinations to idealize the physical properties of the scaffold. Finally, the printing process used can be one of the many currently being used and researched. Leading among them are Ink-jet based and Extrusion bioprinting at this time. However, stereolithography and laser-assisted bioprinting are also utilized depending on the structures you are trying to print[12].

According to the Organ procurement and transplantation network of the United States, as of April 2021, around 3,600 patients were waiting for a heart transplant, approximately 1000 were waiting for a lung donation, close to 12000 require new Livers and a staggering 90,000 are in queue for kidney transplantation. For April 2021, the total number of transplants performed was 13,586. The difference in the demand and supply of organs and tissue to be transplanted is unsettling. This market, of the rest of the world, incapable of procuring necessary, life-saving organs, is who the researchers in this field are trying to save.

Overview of the current state

Tissue engineering(TE) is a multidisciplinary field standing on the cusp of engineering, material sciences, and biological sciences[13]. Traditionally TE is approached through a scaffold-based design. This design is helpful in maintaining the scaffold's structural integrity (For example, Bone) and house the cells for division and differentiation[14]. Some significant factors that affect the overall functionality of the scaffold are,

- Cytocompatible [15]
- Reasonably biodegradable [16]
- Cell protection by the Extracellular Matrix(ECM)
- Should be capable of housing growth factors and proteins
- Young's Modulus
- Porosity
- Cell affinity[15]

The refinement of the structures of these scaffolds has led to the development of some remarkable technologies that are capable of preparing complicated, sustainable structures at the scale necessary.

Bioprinting technologies can be described as computer-aided layer-by-layer deposition of the biopolymer or synthetic polymer in order to create structures to be utilized in regenerative medicine or other biological studies.[17] Since researchers can now slice an object virtually and control the deposition of cells and growth media into these constructs through CAD(Computer-assisted design), we have the ability to prototype organs and tissue rapidly [18].

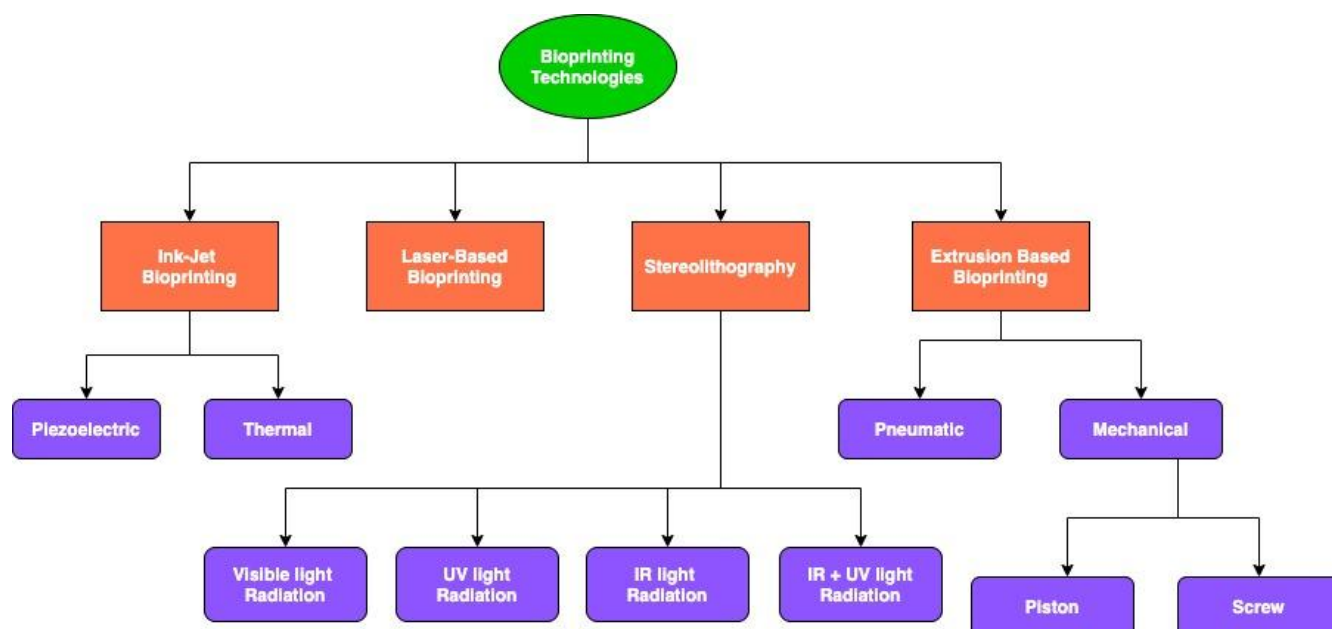


Figure 1.2. Current bioprinting technologies and their subdivisions.

Inkjet bioprinting

Inkjet deposition printers are based on the basic principle of deposition of droplets on paper, based on the 1980's old office printers. This print mechanism can incorporate multiple print heads, hence loading various types of cells and growth factors [19]. The materials are shot onto the paper from the print heads. Thus there is less contamination. This methodology has been used to model complex structures in vitro. Daniela F. Duarte Campos and her team at the Department of Dental Materials and Biomaterials Research, RWTH Aachen University Hospital, Germany, used inkjet printing to fabricate a 3D corneal stromal structure with optical properties similar to the native corneal stroma[20].

The advantage of this type of printing is that it is fast (1–10,000 droplets per second), and its cell viability is greater than 85%. The disadvantage of Inkjet printing is that high viscosity bioinks cannot be used (ideal viscosity of material 3.5–12 mPa/s), and the structural, mechanical stability is weak [21].

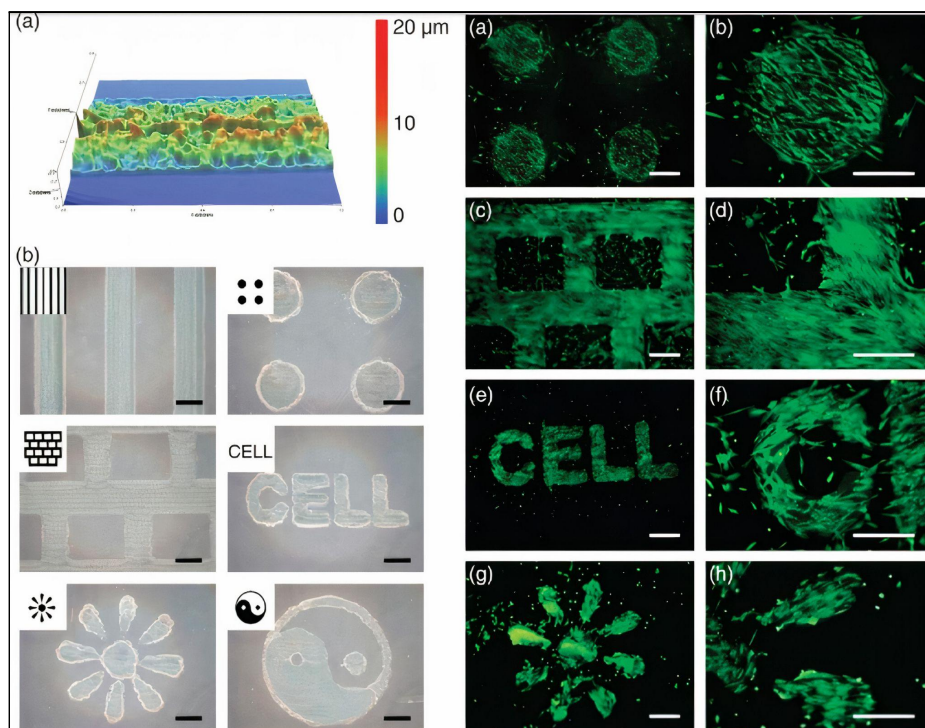


Figure. 1.3. The two-dimensional patterning of PLGA onto the culture substrates.

(I) Optical micrographs of inkjet-printed PLGA patterns. The inserts represent the patterns designed using Adobe Photoshop CS software.

(a) Surface profile of line pattern,

(b) microscopic images of various patterns. Scale bars represent 500 mm.

(II) Fluorescence microscope images of HASCs on PLGA-patterned PS substrates after five days of culture. (a and b) Dot pattern, (c and d) brick pattern, (e and f) “CELL” letter pattern, and (g and h) flower pattern. White bars represent 500 mm

(This figure was adapted from [21])

Laser-assisted bioprinting

Laser-based printing systems were first introduced by Odde and Renn as a way to pattern cell deposition in the year 1999. This is a nozzle-free kind of printing method where the driving force is the laser [22]. The normal mode of operation is that we use a laser to create a light trap for the cells to migrate. Therefore the resolution of the print is in the range of a single cell per droplet. Compared to other bioprinting techniques, laser-assisted printing was not as popular earlier. Nowadays, it is becoming more widely used for the fabrication of tissue for regenerative medicine. In 2013, Stefanie Michael, utilizing Collagen type I(Rat-tail) to print

cell-laden skin tissue using laser-based bioprinting with real in vivo potential[23]. This method of bioprinting holds the potential for contact-free, sterile, and in situ printing of tissue. Laser-based Direct Writing (LDW) is one of the leading methodologies in laser-based bioprinting. It comprises a laser pulse source that creates a bubble followed by a shock wave that deposits the cells from a donor slide onto the collector slide. Other methods include Laser-induced forward transfer (LIFT) and matrix-assisted pulsed laser evaporation direct writing [24].

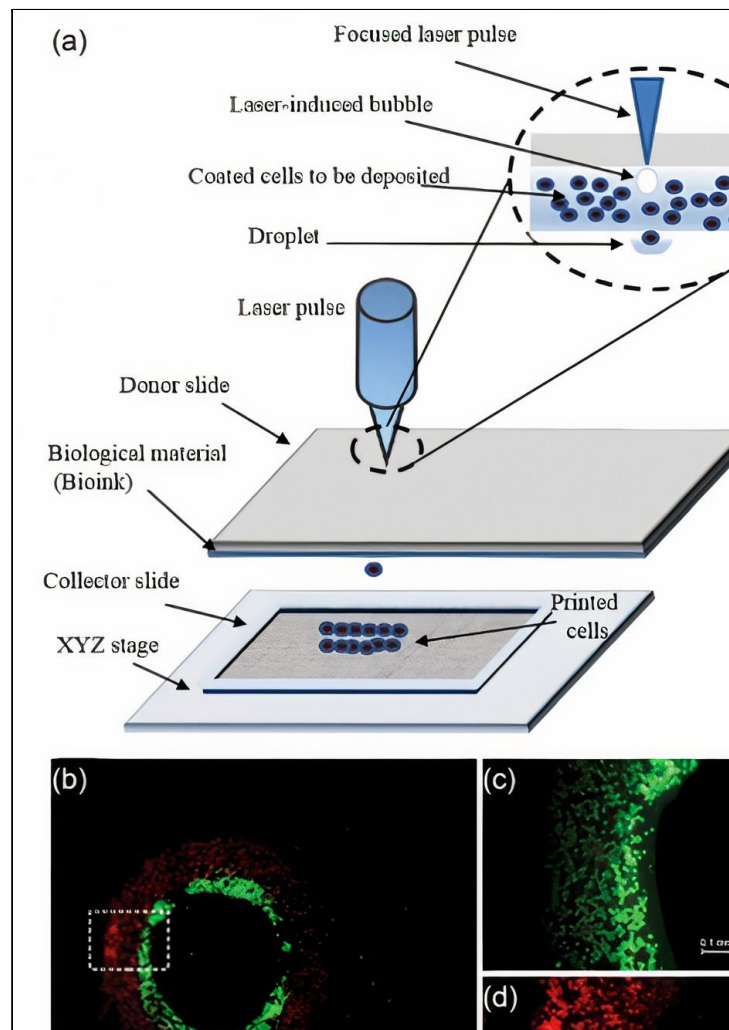


Figure.1.4. Laser-based bioprinting:

- (a) A schematic of laser-based bioprinting (LDW and LAB),
- (b) Different cell types printed in close contact to each other with a high cell concentration,
- (c) Chondrocytes stained with Calcein, and
- (d) Osteoblast cells stained with Dil-LDL Journal[25]

Stereolithography

Stereolithography is a 3 D printing process based on the photopolymerization of a photosensitive resin to create freeform structures. The common process is to expose the photosensitive polymer to UltraViolet radiation through a photo absorptive mask to give the print complex internal structures. This can be very useful in the process of creating internal structures of the heart and lungs one day[26].

Broadly classified SLA can be divided into two categories depending on the light excitation and absorption by the resin; the multiphoton method and the single-photon method. The single-photon method can be further divided as such,

1. Visible light radiation systems
2. Conventional or UV light radiation systems
3. Infrared light radiation systems
4. IR + UV light radiation systems[27]

The major advantage of SLA bioprinting is the high accuracy and resolution of the fabricated structures. For photocrosslinking two, commonly used methods are acryloyl-based photocrosslinking and thiol-ene click reaction. Acryloyl or acrylate hydrogels are a class of photo-cross-linkable biomaterials. These, along with epoxy-based monomers as a combination, are used in commercial SLA machines.[28]. To SLA print bio-organic structures, Kathryn E. Drzewiecki, Juilee N. Malavade, and their team developed Collagen methacrylamide (CMA), which, like collagen, forms fibrils but, in contrast, is photocrosslinkable and thermoreversible. This allowed them to utilize masks to create the desired complex structures and be able to remove the undesired structure by cooling the print[29].

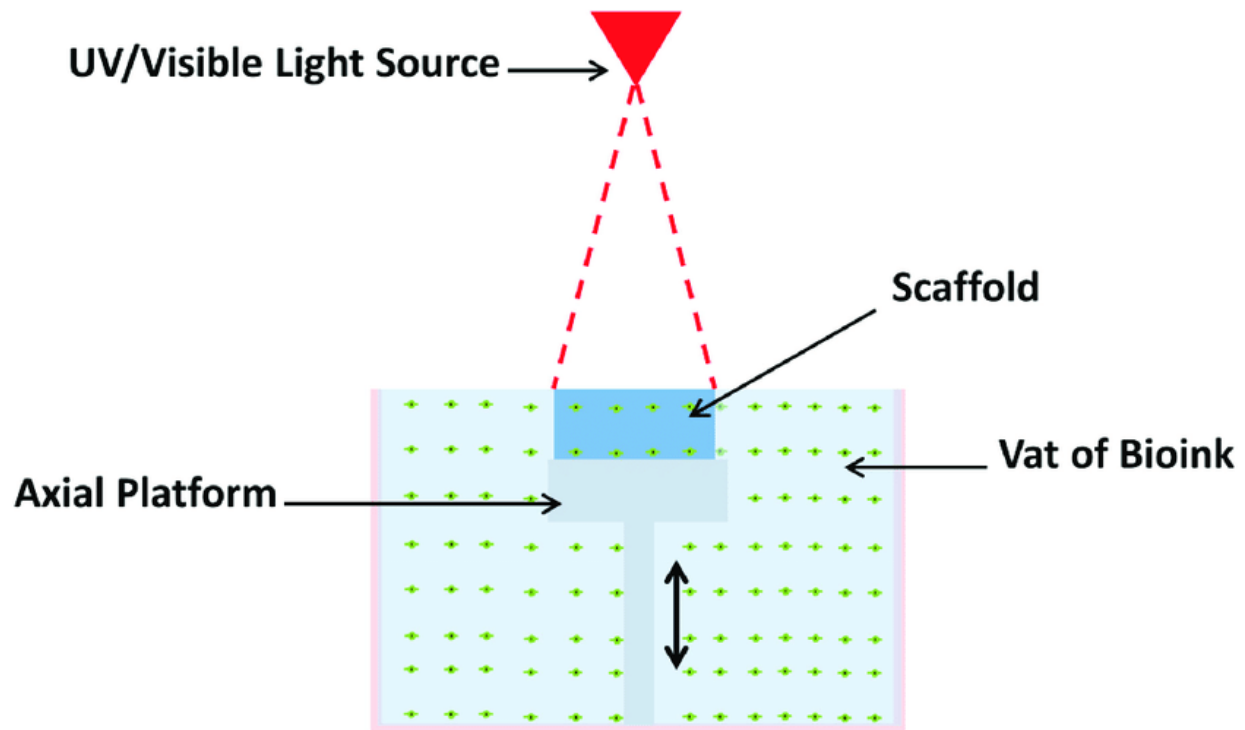


Figure .1.5.Schematic of Stereolithography Bioprinting. Photopolymerization occurs on the surface of the vat, where the light-sensitive bioink is exposed to light energy. The axial platform moves downward the Z-axis during fabrication. This layer-by-layer technique does not depend on the complexity of the design,insteadr on its height [30]

Extrusion bioprinting

Fused deposition modeling (FDM) along with SLA has been in activity since 1988~1989[31]. Following this, additive manufacturing (AM) guided through 3D software opened up an era of inhouse manufacturing.

Extrusion printing uses material crosslinking mechanisms, which can broadly be divided into the following [32]:

1. Photo-crosslinking
2. Chemical crosslinking
3. Physical crosslinking

Extrusion bioprinters can print structures based on CAD drawings and influence the exact structures and properties that we then place the cells in [33]. Extrusion printing is based on the concept of using pressure to extrude cross-linkable monomers to get a polymeric structure.

With the development of biological tissue in Vitro, it is gaining pace in the race of innovation, and extrusion printing seems to be the most effective[34]. Yongbok Kim and his team at the Department of Biomechanics Engineering, College of Biotechnology and Bioengineering, Sungkyunkwan University (SKKU), Suwon, South Korea, worked on a strategy for the fabrication of mechanically stable, cell-laden porous scaffold with the potential for bone regeneration[35].

General extrusion-based printing can be classified according to the activating force of the extrusion. These can be pneumatic, piston, or screw-based mechanisms that govern the extruded material. Creating microchannels for the purposes of vessels, arteries, veins, and required seeding of stem cells in structured microchannels for guided growth is much more convenient compared to other methods[36]. Researchers have also successfully printed a liver model in which the primary hepatocytes retained their functionality for two weeks and responded appropriately to toxic substances[37].

In this kind of bioprinting, the printing material generally consists of a cell-laden hydrogel that can flow smoothly through the extruding needle. Unlike Inkjet printing, there is no individual droplet creation. Instead, a continuous stream of bioink is created.

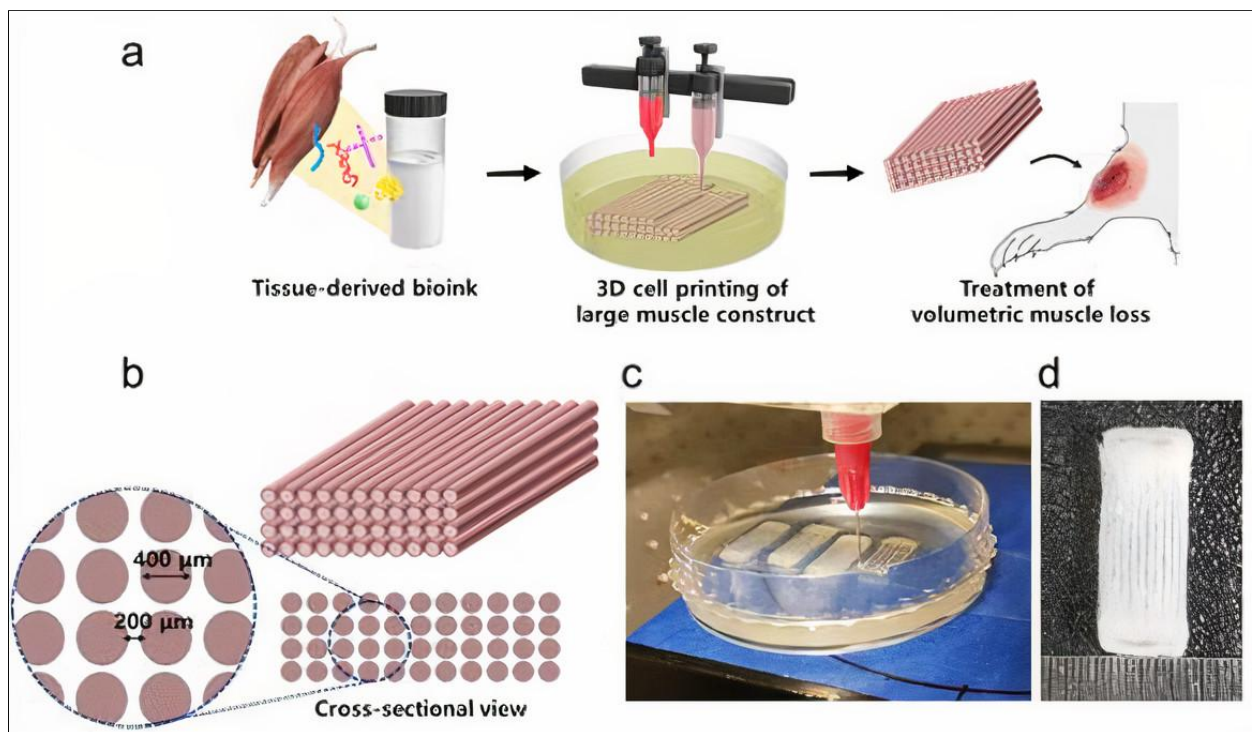


Figure.1.6. (a) Schematic illustration of the decellularized extracellular matrix (dECM) bioink preparation, muscle construct fabrication, and volumetric muscle loss (VML) treatment. (b) Design of muscle construct. (c) 3D cell printing of muscle construct using a granule-based reservoir system. (d) 3D cell printed muscle construct. Figure adapted from [38]

Hydrogels and Bioink

Hydrogels are typically polymers that are extensively used in bioengineering and biomanufacturing. They are used as cell delivery vehicles, capable of providing the cells a 3D environment similar to natural tissue[39]. Hydrophobicity is one of the main functions that determine the effectiveness of a hydrogel in encapsulating the cells[40]. Hydrogels can be naturally derived, such as collagen, Chitosan, alginate, and fibrin, or synthetically derived polyethyleneglycol and poly(vinyl alcohol)(PVA). Synthetic hydrogels often lack bio functionality, whereas natural hydrogels like collagen are very cell compatible[41].

The development of an ideal biomaterial for printing is one of the most significant challenges of the field. The ink needs to fulfill the requirements of the cells as well as the mechanical strength of the tissue. “Bioink,” which is the printing material, is effectively hydrogels that contain cells that are required for regeneration. An effective bioink should be capable of manufacturing robust and strong constructs with tunable tissue-matching mechanics. Its gelation should be adjustable to give the desired mechanical properties. Also, biocompatibility and its ability to withstand chemical processes for tissue-specific needs are important characteristics of bioinks[42].

Natural, synthetic, and a combination of the two types, polymer-based bioinks are already being tested and researched all over the world. Among the natural polymers, Alginate based bioinks with Cartilage progenitor cells(CPCs), or Human umbilical vein SMCs have both been utilized for the development of Vascular tissue[43]. Aortic root sinus SMCs and aortic valve leaflet interstitial cells along with Gelatin have been used in extrusion printing for the development of an Aortic valve [44]. Synthetic polymers like PCL, along with chondrocytes and osteoblasts, have been used to extrusion print osteochondral tissue[45].

Collagen

Collagen is a natural polymer that is found in abundance in the Extracellular matrix (ECM). Its fundamental structural unit is a 300 nm protein consisting of 3 braided α -subunits of 1050

amino acids in length. Although collagen has 29 variants, 90% of the collagen found in adult mammals are Type I, Type II, and Type III. “Collagen is a hierarchical biomaterial that is self-assembled into fibrils (containing numerous structural units) of ~1 cm length and ~500 nm in diameter (using type 1 Collagen as the archetype)”[46]. This gives rise to a triple Helix macromolecular structure which has decent three-dimensional strength. On exposure to heat energy from the surroundings, the H-bonds maintaining the helical structure break and give rise to a denatured and disorganized mass of Gelatine.

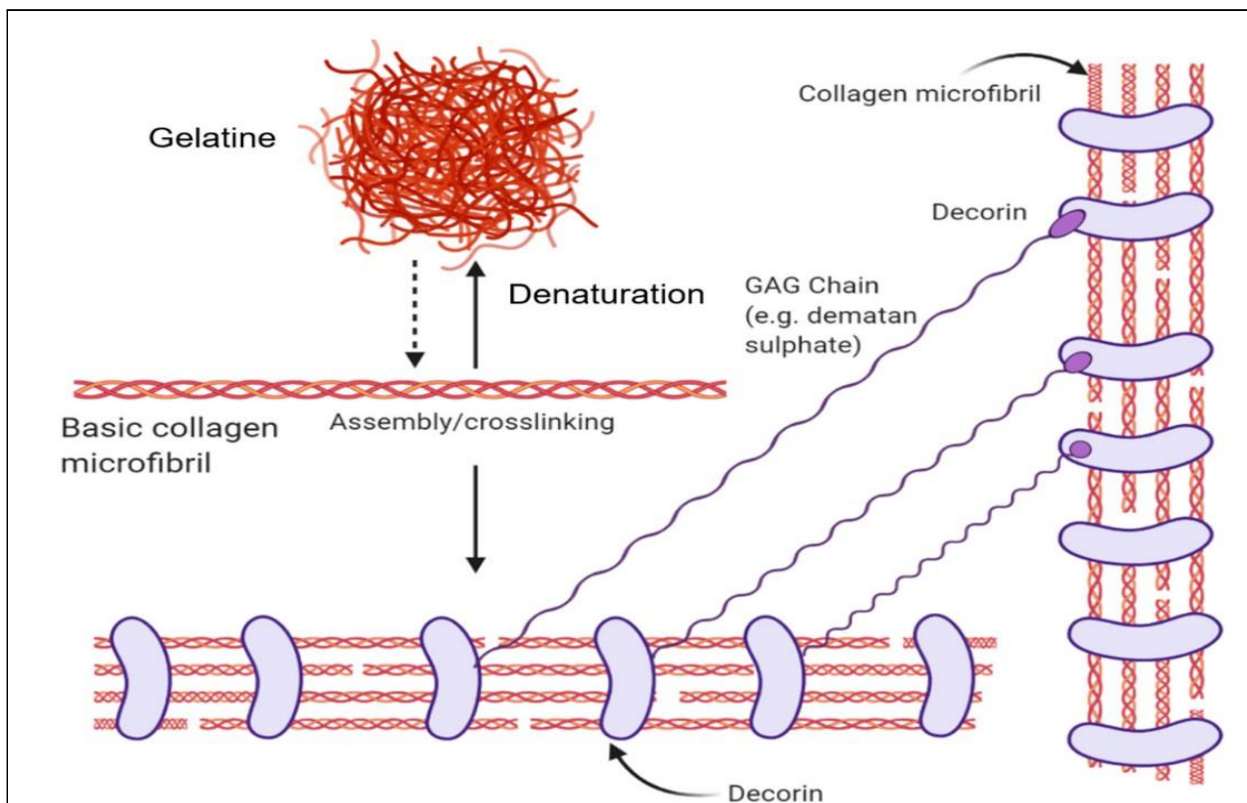


Figure.1.7. The structural forms of collagen and their native interactions. The basic collagen unit is a triple-helix microfibril that denatures into gelatine or can be assembled into collagen fibrils. Decorin proteins wrap around collagen fibrils in their native context and bind with glycosaminoglycan chains such as dermatan sulphate. [47]

Poly-caprolactone (PCL)

Polycaprolactone is a thermoplastic polymer that is biocompatible. It has been developed and optimized for 3D printing purposes. PCL has been used in implants, and more recently, as a

component in bioinks to provide more support. Due to the agreeable melting point in the range 59-64°C and the density of 1.10-1.15 g/ml, it makes a valuable material for molding scaffolds.

Its structure of PCL is slightly crystalline and also highly hydrophobic. The polymerization of ϵ -caprolactone assisted with a catalyst like stannous octoate[48].

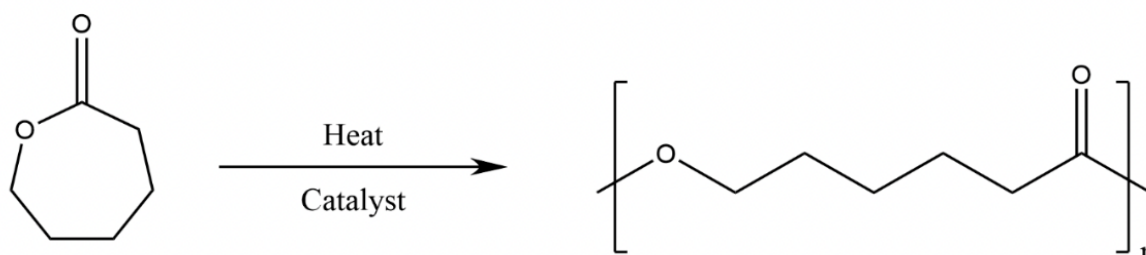


Figure.1.8. Polymerization of PCL by the opening of the cyclic form in the presence of heat as a catalyst[49]

Types of cells in bioinks

A controversial field in some countries to be working in, Stem cell technology can cure multiple illnesses actively. Stem cells are cells found all over the body, in the bone marrow, the adipose tissue, liver tissue, and they can differentiate into a variety of cell types. This multipotency is an attractive quality for the formulation of bioink. These cells can be used in conjunction with hydrogels to provide the attributes we desire in the scaffold.

Stem cells that can be used as a component in bioinks can be divided into mesenchymal stem cells (MSC), Embryonic Stem Cells(ESC), Induced pluripotent stem cells (iPSCs)[50].

Mesenchymal progenitor cells are stem cells that are capable of differentiating into adipocytes and chondrocytes. For a long time, it was believed that the stem cells were only capable of differentiating into the tissue they were extracted from, but over the years, methods were adopted that allowed them to differentiate into unrelated tissue like neurons, myotubes, tenocytes, and hematopoietic-supporting stromal cells [51]. For example, Hematopoietic stem

cells derived from the bone marrow or peripheral blood vessels are capable of not only differentiating into not only blood but also liver cells [52].

Embryonic stem cells are pluripotent in nature, which implies that they can differentiate into all mature somatic phenotypes on being introduced to appropriate signals. ESCs are derived from the inner cell mass of blastocysts. The researcher removes the trophectoderm and retrieves the inner cell mass, which forms a new line of Embryonic Stem Cells for stem cell research [53]. These ESCs, given the right conditions, appear to be immortal and capable of unlimitedly dividing and creating more ESCs and maintaining a normal Karyotype [54].

Induced pluripotent stem cells are derived from skin cells or blood cells. These cells are reprogrammed to revert to a pluripotent embryonic stem cell-like state that allows differentiation into any type of cell needed by a patient. iPSCs are actively being used in the research of regenerative medicine and drug discovery. It, in turn, solves the controversial aspect of retrieving ESCs from human embryos[55].

Aims of Thesis

Our work here builds on the knowledge of a multitude of researchers who are actively working on perfecting bioprinting technology. What we aim to accomplish through this project is a better understanding and optimization of the printing process on nanofiber substrates for the purposes of regenerative medicine. The paper intends to encapsulate the following points essential for the proper execution of the project;

1. We will design a mounting fixture for the planar nanofiber substrates for a 3D bioprinter. The nanofiber substrate to be used will be PCL or collagen-based.
2. The fixture design will be optimized to work in a sterile environment in a laminar box and verify that it can withstand the sterilization process using an Autoclave.
3. The tool path generation related to the fixtures and attached nanofiber needs to be optimized.
4. Finally, the design will be verified through cell experimentation and analysis. The cell experimentation will involve human or porcine primary cells printed in porcine-based collagen on the nanofibers.

The fixture needs to be designed to hold two 20x20 mm in a well-like structure to hold the culture medium or crosslinking agents. It also needs to be composed of material that can sustain the high temperatures of an autoclave.

The travel path of the extruder has to be mapped and optimized to avoid collisions with the bed frame (Designed fixture) and can efficiently print two constructs sequentially. The printing and movement of the extruder will be concentric and continuous. This movement of the tool path needs to be tested and verified before moving on to the next step.

On completion of the verification, we will print on nanofiber substrates with a collagen-based bioink containing Adipose tissue-derived porcine stem cells (pASCs).

Final cell analysis will be done based on image processing and trainable classifiers to check the condition of the embedded cells in the bio-printed structure.

2. Methods

2.1 Development and fabrication of the fixture.

Design requirements:

- The fixture dimensions were set on the initial CELLINK bioprinter with the depression in the print bed of 128x85 mm.
- The base plate needs to contain two nanofiber sheets of 20x20mm.
- Two clips are needed to be designs that will hold nanofiber sheets together
- Structure needs to be in the form of a well so that it can contain a liquid-phase crosslinking agent
- For the system to be watertight, silicone gaskets will be used of 1mm thickness
- Bolts need to be as low as possible in the structure so as the bed structure does not get in the path of the extruder.

The first design proposed was developed on Shapr3D Software shown in Fig.2.1c., Designated **Version 0**.

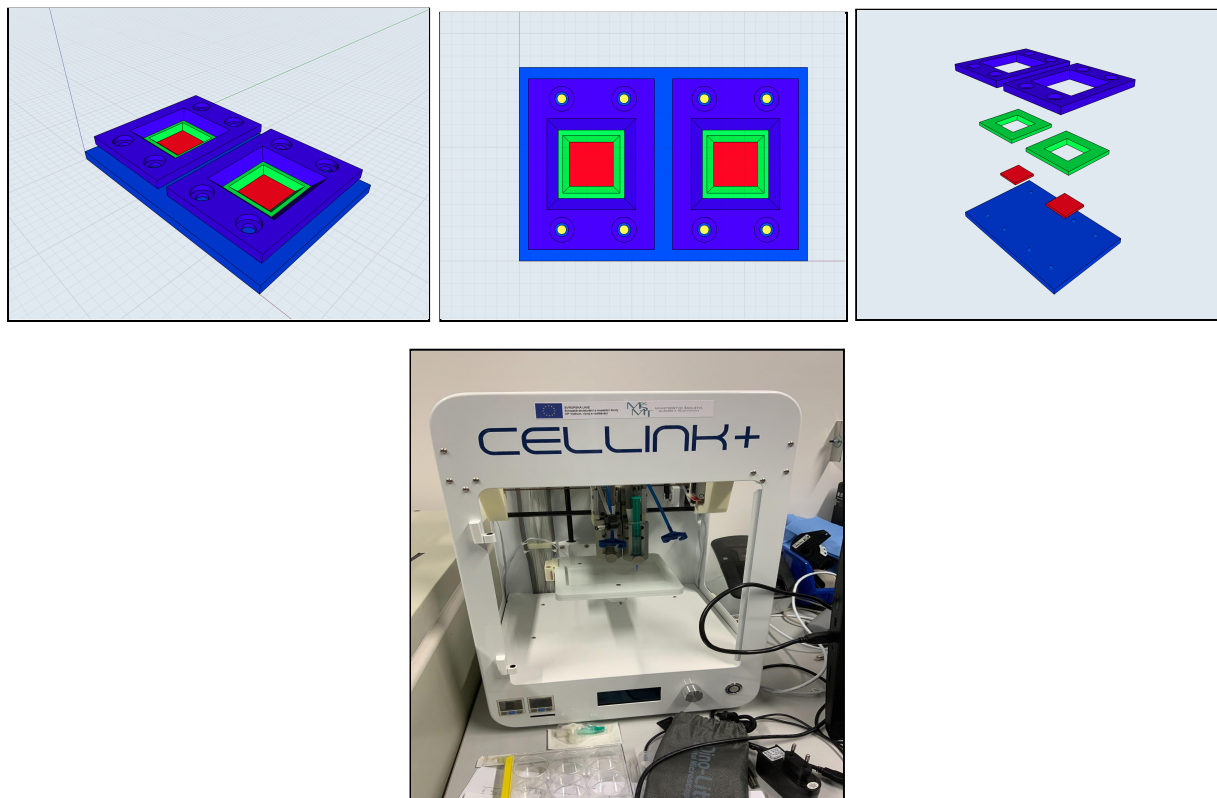


Figure. 2.1. First design in Shapr3D for the CELLINK+ bioprinter

On review, changes to the designs were executed on Autocad fusion 360 in the laboratory at the Faculty of Biomedical engineering. Revisions to the designs

- The initial design had clip dimensions of 46mm x 75mm, and the inside edge was 16mm.
- The chamfer went all the way from top to bottom of the clip. The chamfer itself was 5mm.
- The holes for the screws were not symmetrical to the center of the printing squares.
- There were no holes for aligning the extruder point and the centers of the printing squares.
- The silicon gasket was 40mm by 40mm with a cutout square in the center 16x16
- the holes for the bolts did not go all the way through the baseplate.

1. Fixture design 1 Version 1 (B1V1)

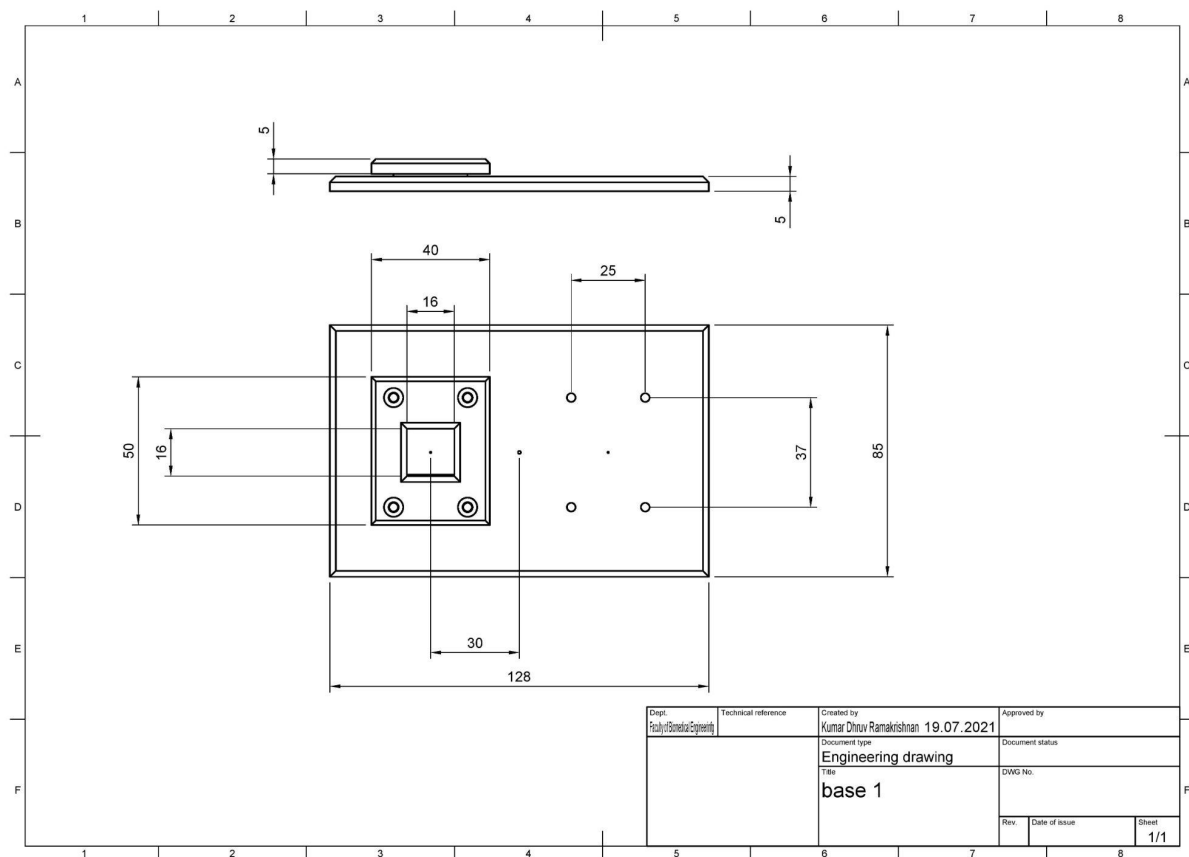


Figure.2.2. Fixture design 1 Version 1 (B1V1)

The above figure, figure.2.2 contains the first base plate design to hold the nanofibers. The base dimension for this version was 128x85mm. These measurements were taken, and a circle

of 0.5mm diameter was placed at the center for the reference of the 3D bioprinter shown in Fig.2.1

- The two clips will screw onto the base to hold the nanofiber sheets in place steadily for the printing mechanism. The gaskets are made out of silicon to create a watertight well to contain the calcium bath for crosslinking.
- The outer dimensions for the clips are 40mm x 50mm, and the Internal square is 16mm per side.
- The 1mm silicone gaskets have an outer dimension of 25mm x25mm, and inner dimensions are 16mm x16mm.
- Markings are aligning the clips and the silicone gaskets on the base plate, and both are symmetrical to the center.
- There are 0.5mm diameter holes on the center of the baseplates and the centers of the printing square which are each 30mm away from the center of the baseplate.

2. Fixture Design 2 Version 1 (B2V1)

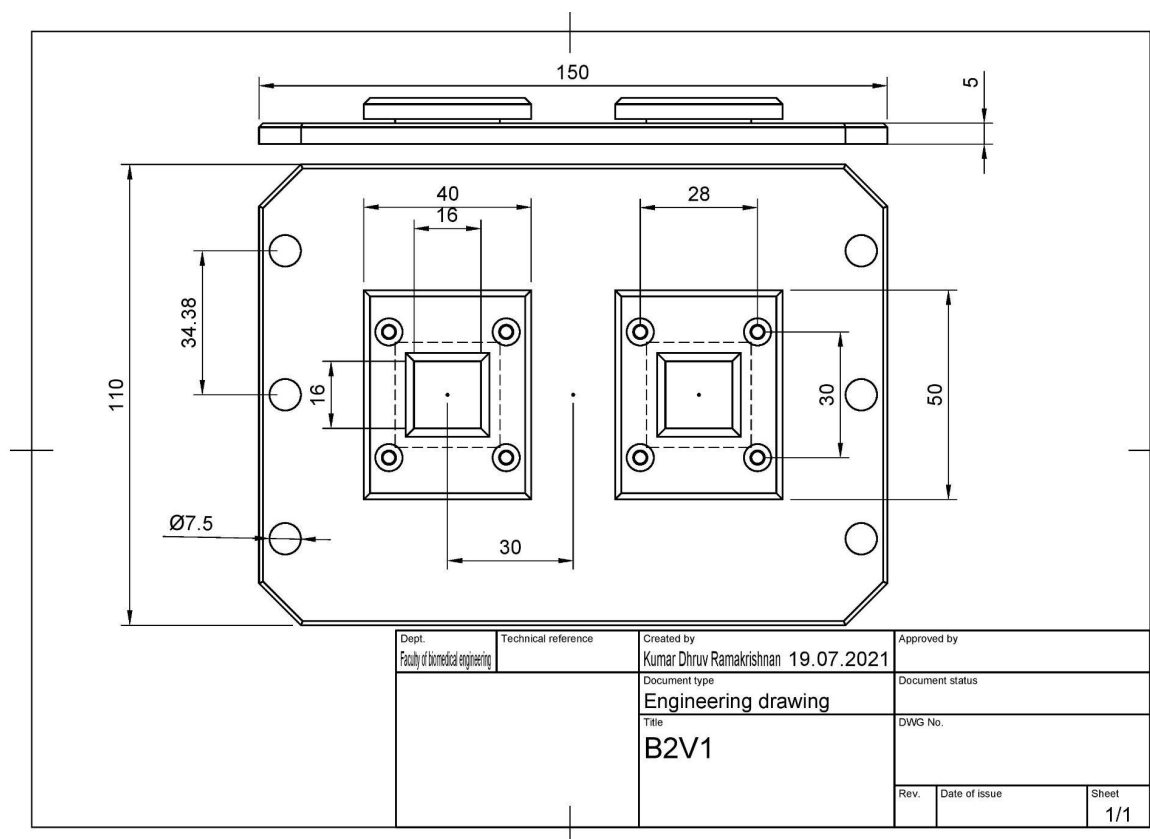


Figure.2.3. Fixture Design 2 Version 1 (B2V1)

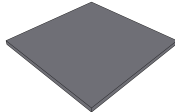
In figure 2.3 the second type of base plate design to hold the nanofibers. It was designed to settle on top of an existing structure on the bioprinter. The dimensions for the base are 150mm x 110 mm. A circle of 0.5mm diameter is placed at the center for the reference of the custom 3D bioprinter developed by professor Matejka.

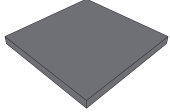
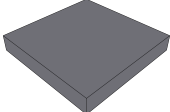



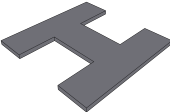
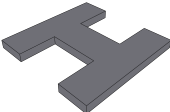
- The two clips will screw onto the base to hold the nanofiber sheets in place steadily for the printing mechanism and the gaskets made out of silicon to create a watertight well to contain the crosslinking agent.
- This fixture sits on a pre-designed bed with bolts holding it in place.
- The design is similar to the previous fixture design with a center hole of 0.5mm, 55mm from the bottom.
- Similarly, two 0.5mm holes are at the center of the printing squares on top of which the gasket and the clip reside.
- The Center of the base plate is 75mm from the sides.

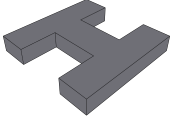
2.2. Preparation of Printing constructs and optimization of the tool path

For the purposes of comparison of the effect of shape and structure on the cells embedded in the Bioink, we optimized the tool path for constructs of Circle, Square, and H shape. As the printing well in the fixture spans 16x16mm, the constructs were proposed to be 13x 13mm. On consideration, Given that the inner dimension of the nozzle was 1mm, the clearance between the outer dimensions of the nozzle and the clip's inner wall was approximately 0.5 mm. Therefore the constructs were reduced in size to have a maximum dimension of 13 mm.

Table. 2.1. Dimensions of constructs to be printed

<i>constructs</i>	<i>dimensions (mm)</i>	<i>Estimated time of print (s)</i>	<i>concept images</i>
Square	0.5 x13 x13	45	

	1 x13 x13	1m	
	2 x13 x13	2m	
Circle	0.5, 13 \varnothing	40	
	1, 13 \varnothing	1m	
	2, 13 \varnothing	2m	
H - shaped	0.5 x13 x13	27	
	1x13 x13	54	

	2	1m	
--	---	----	---

2.2.1 Creating configurations for the custom bioprinter

1. Customization of the Printer profile settings for the two fixtures

The three Dimensional bioprinting machine developed by Ing. Roman Matejka PhD. at The faculty of biomedical engineering was the system on which the settings were based.

The slicer software we use for this purpose is PrusaSlicer which is an open-source software capable of handling multiple prints and along with the ability to create custom profiles for new printers. The flavor for the formula G-code is set to “Repetier,” which is one of the most common firmware used for 3D printing. Repetier-Host is a 3D printing application developed by Hot-World GmbH & Co. KG. It is an easy-to-use, free application that is compatible with Prusaslicer and Slic3r.

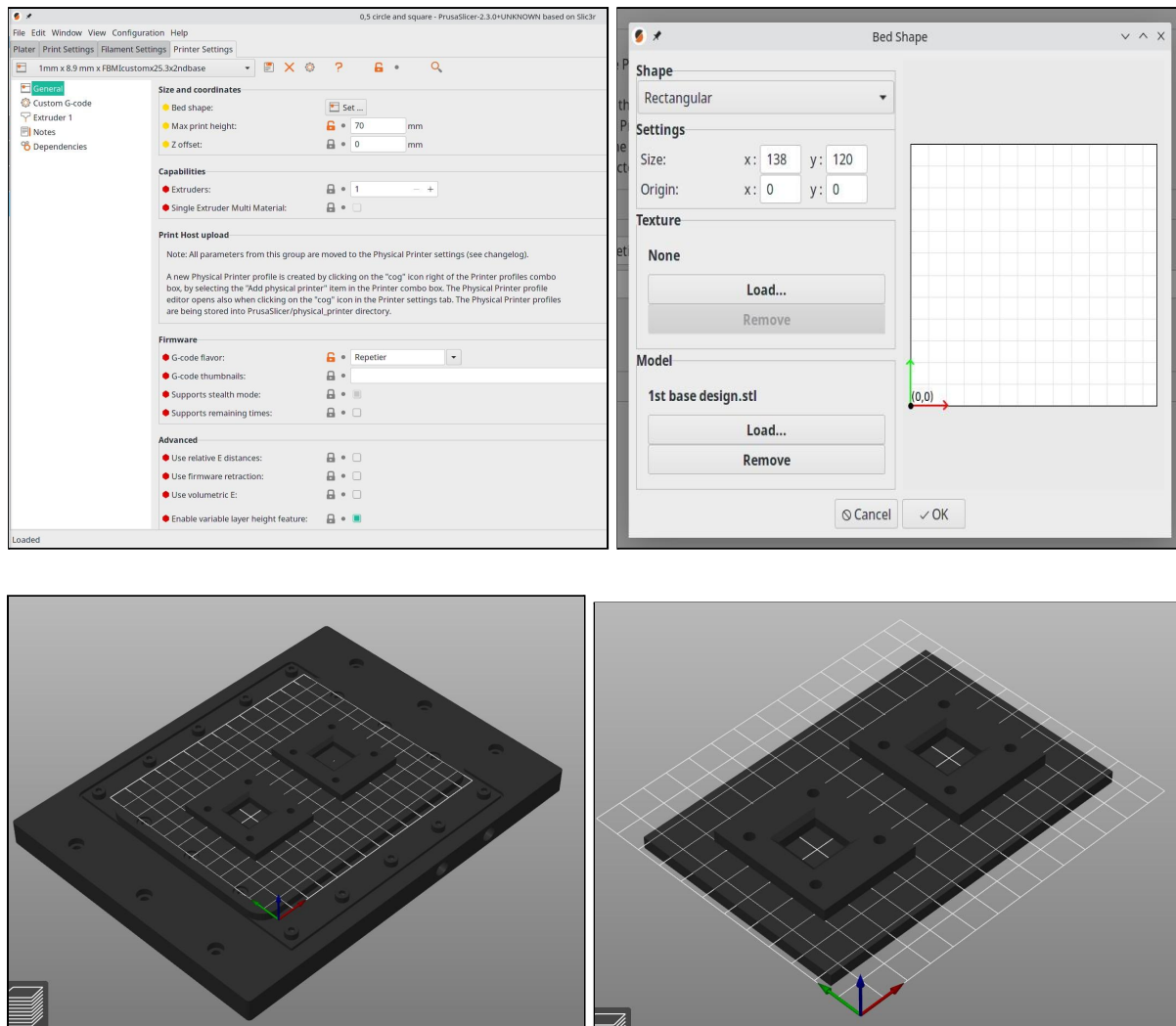


Figure.2.4. Bed profiles and printer settings

The custom-designed bed profile is introduced to the Prusa slicer through the configuration wizard. This setting can be accessed through the general settings of the printer settings tab.

- The center of the bed profile is at 69,60. And the origin is placed at the lower-left corner.
- The models from B1V1 and B2V2 are loaded (Format: STL) from the model box in the Bed shape tab.
- The origin is placed at the lower-left corner, and the bed size is set to 128 x 120.
- The maximum height for the print profile set for the custom printing is 70mm.

The optimization needs to be done for a single extruder, which was also set in the general category of the printing settings.

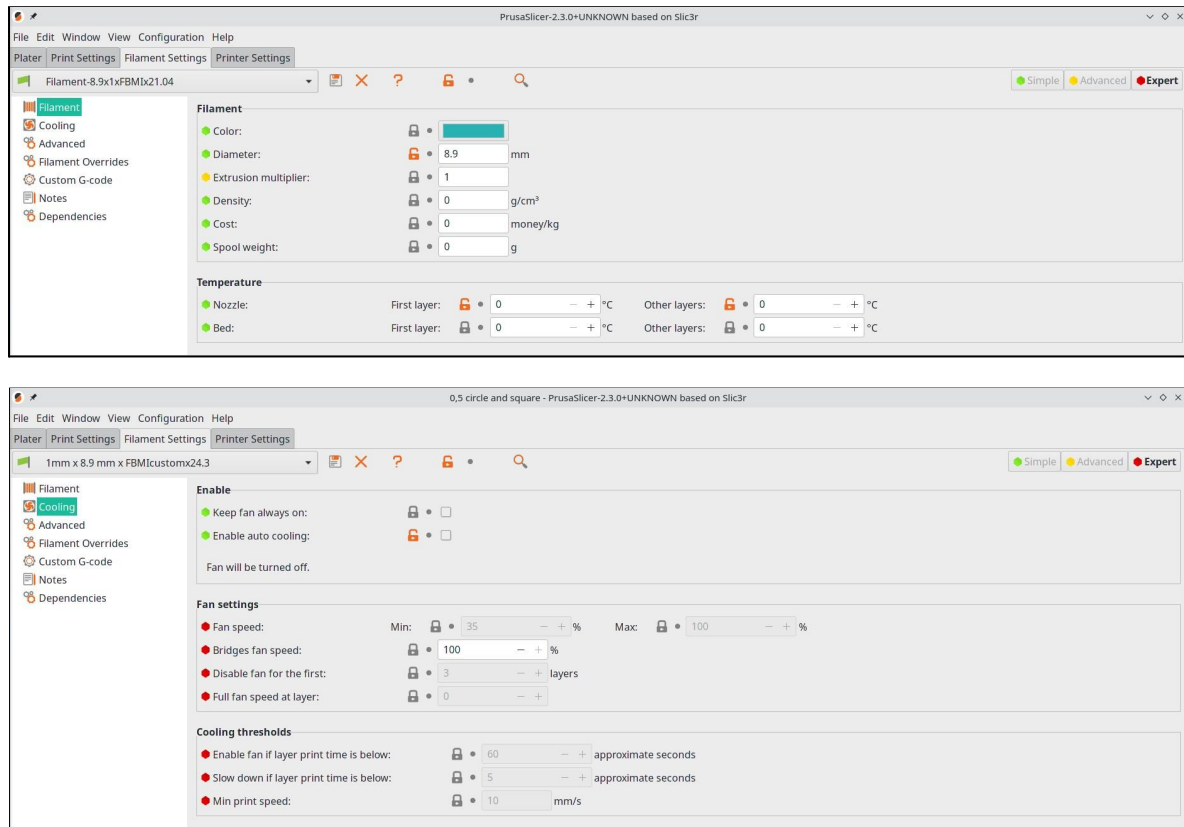


Figure.2.5. Filament settings and fan settings.

- The single extruder system employed in the bioprinter is a syringe-based extruder with a cylinder diameter of 8.9mm and the extruder diameter of 1mm.
- The temperature settings are turned off since the bed and the nozzle is not heated. The corresponding settings are made in the temperature box in the filament category in the filament settings.

2. Tool Path Optimization

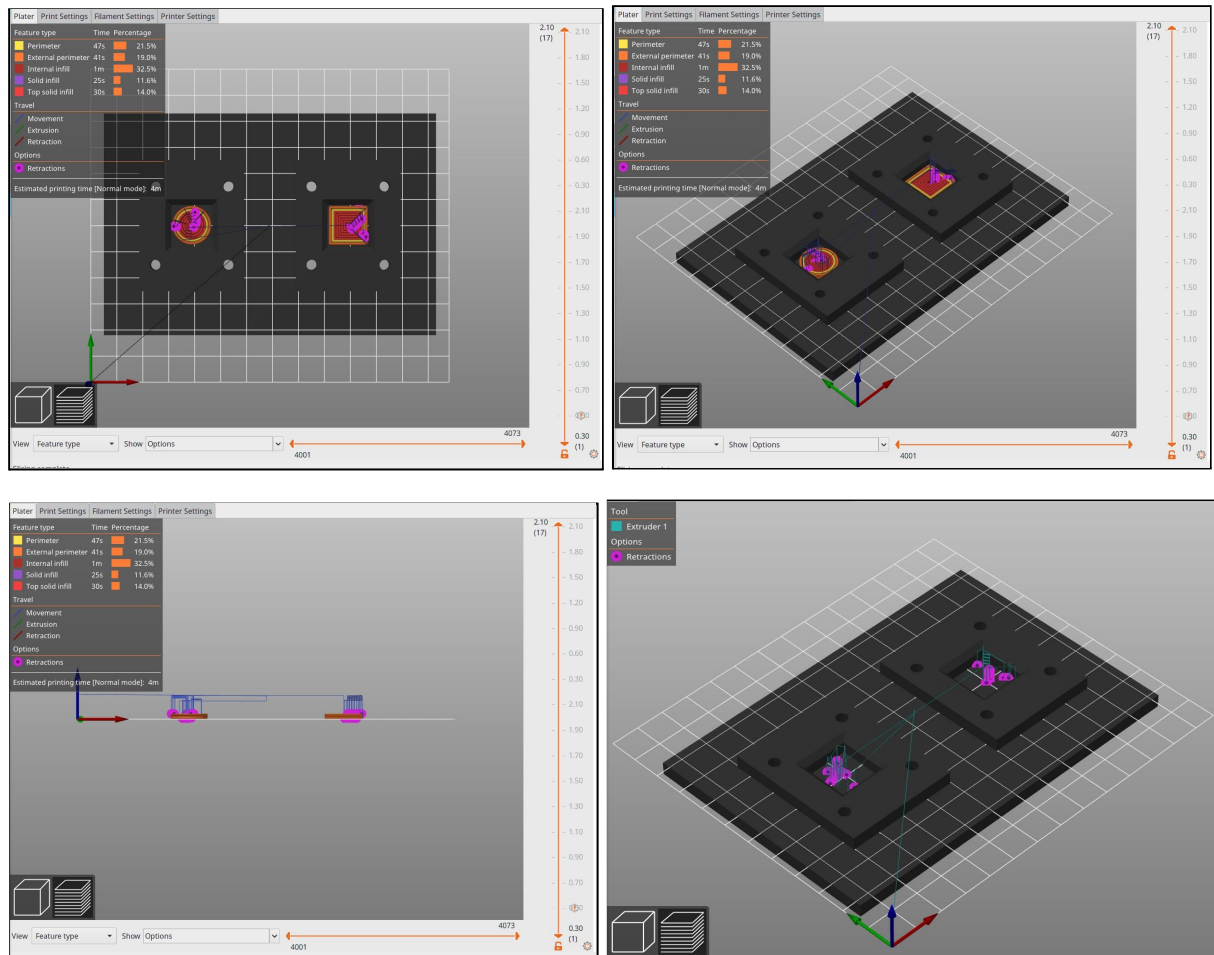


Figure. 2.6. Visualization of the travel path and retractions

The travel path of the extruder tool can be visualized through the features options at the bottom of the page on the platter tab. We can observe in figure.2.6. the tip of the extruder rises to a height of 7mm, avoiding the bed profile entirely and homing in on the center. When it starts printing, it prints in the order it presents on the left-hand dialogue box on the platter tab.

The retractions are visible in pink, showing the retractions for the constructions of the perimeters first.

- Retraction settings are set in the Extruder1 option in the Printer settings tab.
- The length given as 1 denotes the amount of filament being pulled back when retraction is triggered.
- Lift Z refers to the lift of the extruding tool. The z value of the extruder is quickly raised every time a retraction is triggered.
- Retraction speed is set to 40 mm/s, which is also the de-retraction rate is set to zero.

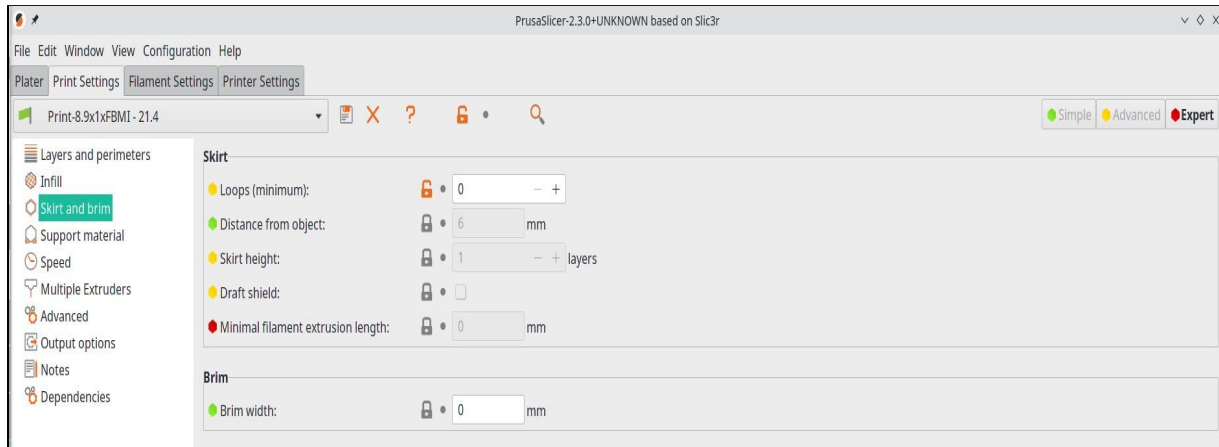


Figure. 2.7. Skirt and Brim.

The purpose of the brim is to create an adhesive sacrificial layer between the construct and the printing plate for when the print is taken off. However, we were printing structures that needed to adhere to the nanofiber substrates at the bottom of the wells. Hence the option for Brim needs to be deactivated.

The skirt is the boundary line around the constructs. These vary based on the shapes of the constructs and run the risk of collision with the bed profile.

Therefore, in the skirt and Brim option of the Print settings tab, the loop option in the Skirt box and the Brim width in the Brim box are set to 0, disabling the functions.

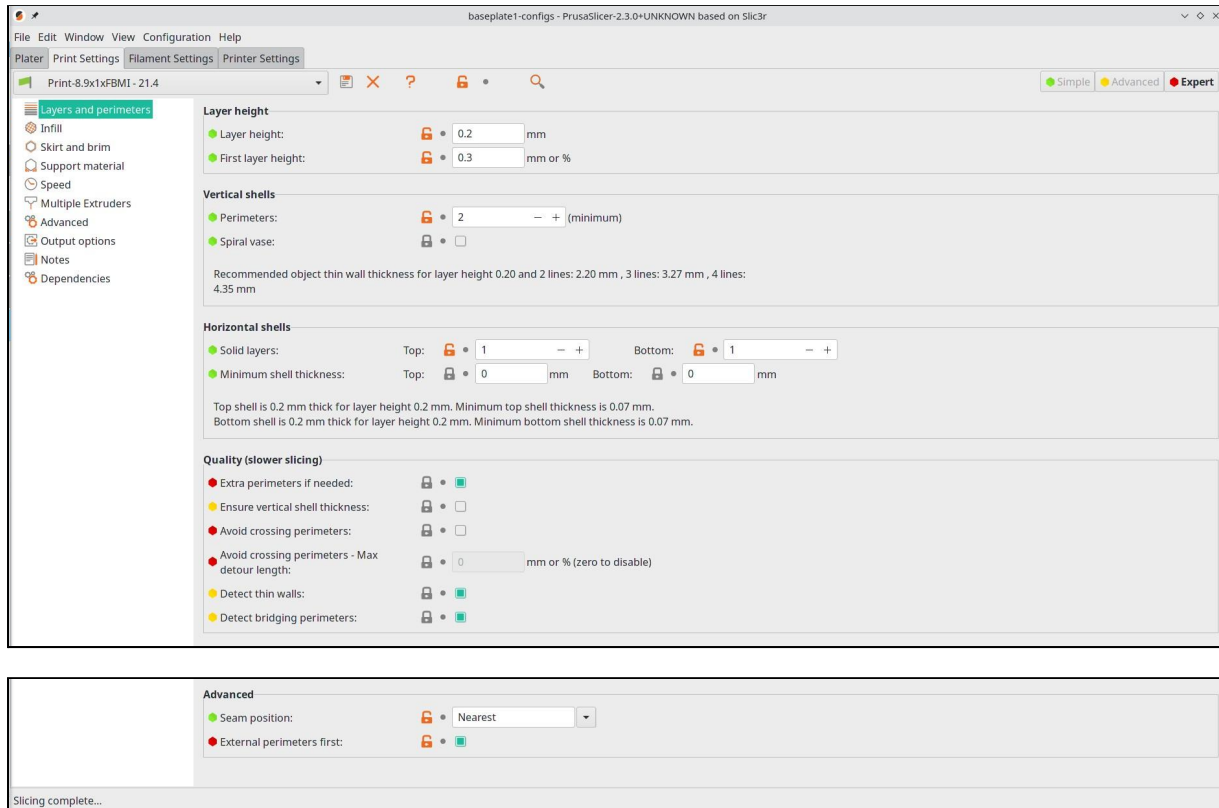


Figure. 2.8. Layers and perimeters settings

- The first layer thickness is set in the Layer height section of Layers and Perimeter in the Print settings tab. The height of the first layer is set to 0.3 mm, and every consequent layer is set to have a height of 0.2 mm. Perimeter

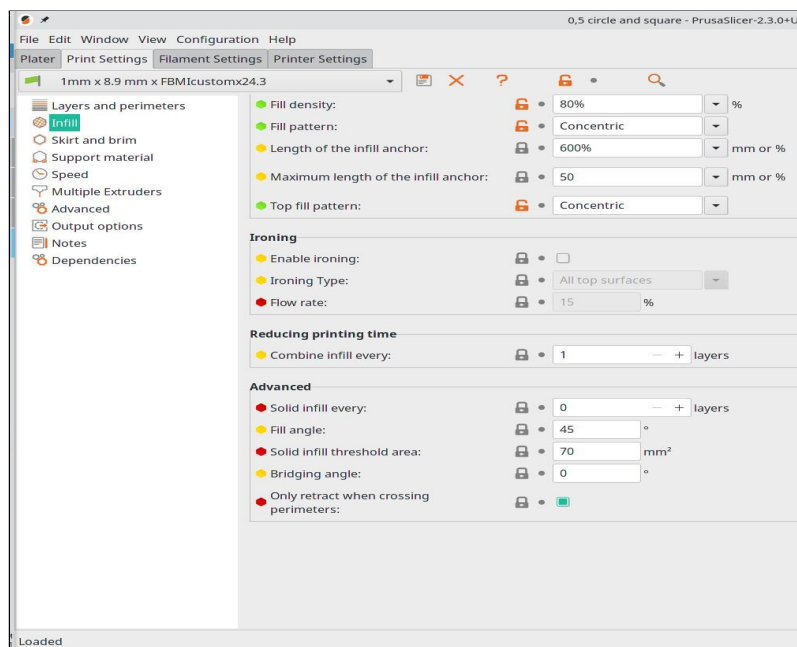


Figure.2.9. Infill settings

- The infill density was set to 80 %, and the patterns of infill were chosen to be concentric. The Fill pattern, Top-fill pattern, and Bottom fill pattern are set as concentric, and the biprinter will print the perimeters first as indicated in the Advanced section of the Layers and parameters category.

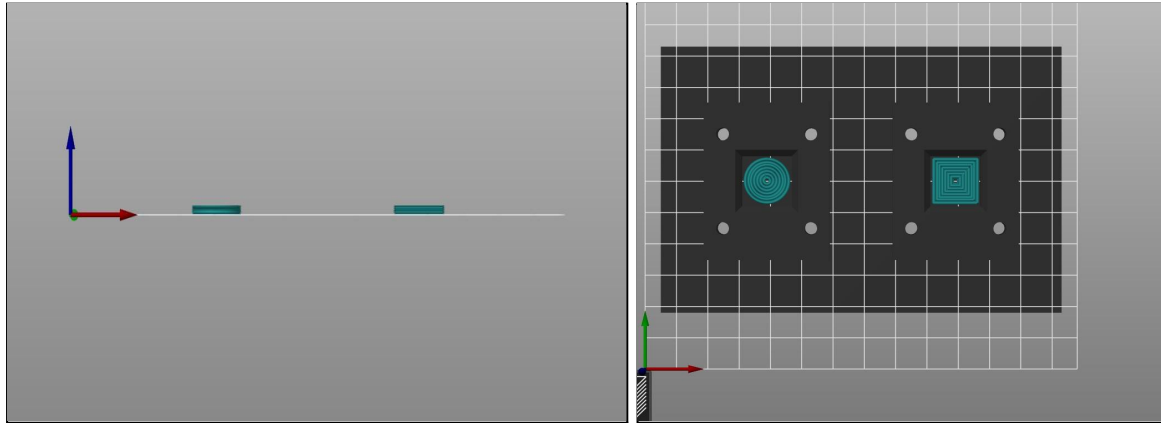


Figure. 2.10. Concentric print with infill first mode

In order to give a homogenous distribution, the printing strategy has been to create concentric extrusions. To support the structure properly due to the low viscosity of the extruded material, I set the infill to be extruded first when starting and the number of loops of the perimeter is set to 0. and then the infill is filled at 80% starting from the outer edge going to the center, with one layer of solid fill on top.

The platters contain the visualized form of the print bed and print constructs. You can see in figure.2.10. , on the left is a window containing all the print profiles, which can be hidden or shown using the icon to generate the G-code of the constructs you need. This is a one-time addition that can be put into fast alterations to the infill and layer heights. The G-code for any combination can be chosen and generated for printing.

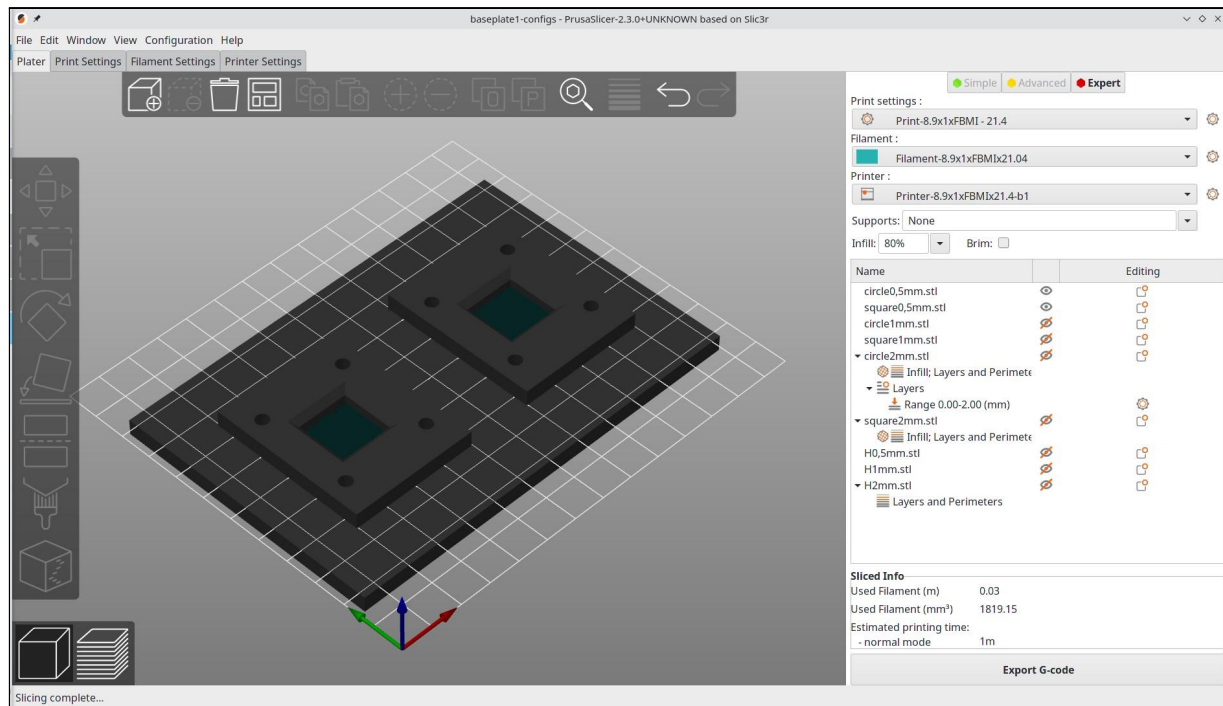


Figure.2.11. Platter containing all the print constructs

3. Revisions based on section 2.4.

1. An STL file for the B2V2 design was uploaded as the bed profile.
2. All the speeds were set to a constant 10mm/s
3. Increased the number of the perimeter to 10 (more than the number of loops on the structure) and disable “infill before perimeters” as shown in fig.2.11. This helps generate concentric prints.
4. The Infill density was changed from 80% to 100%
5. The diameter of the syringe was changed to 9.75 mm
6. The start and end G-code was edited for the Prusa-slicer generated G-code.

i. **Start Code :**

```
;G28; Home all axis

M42 P5 S1;

M302 S1;
```



```
G92 E0;  
  
G1 Z10 F600; go to z=10mm  
  
G1 X68 Y58 F600;  
  
G1 X38 Y58 F600;  
  
G92 E0;  
  
G21 ; set units to millimeters  
  
G90 ; use absolute coordinates  
  
M83 ; use relative distances for extrusion
```

ii. **End Code :**

```
G1 Z27 F600;  
  
G1 X136 Y116 F600; Get extruder out of the way.  
  
M42 P5 S0;  
  
G91 ; Relative positioning  
  
G90 ; Absolute positioning  
  
G92 E0 ; Reset extruder position  
  
M84 ; Turn steppers off
```

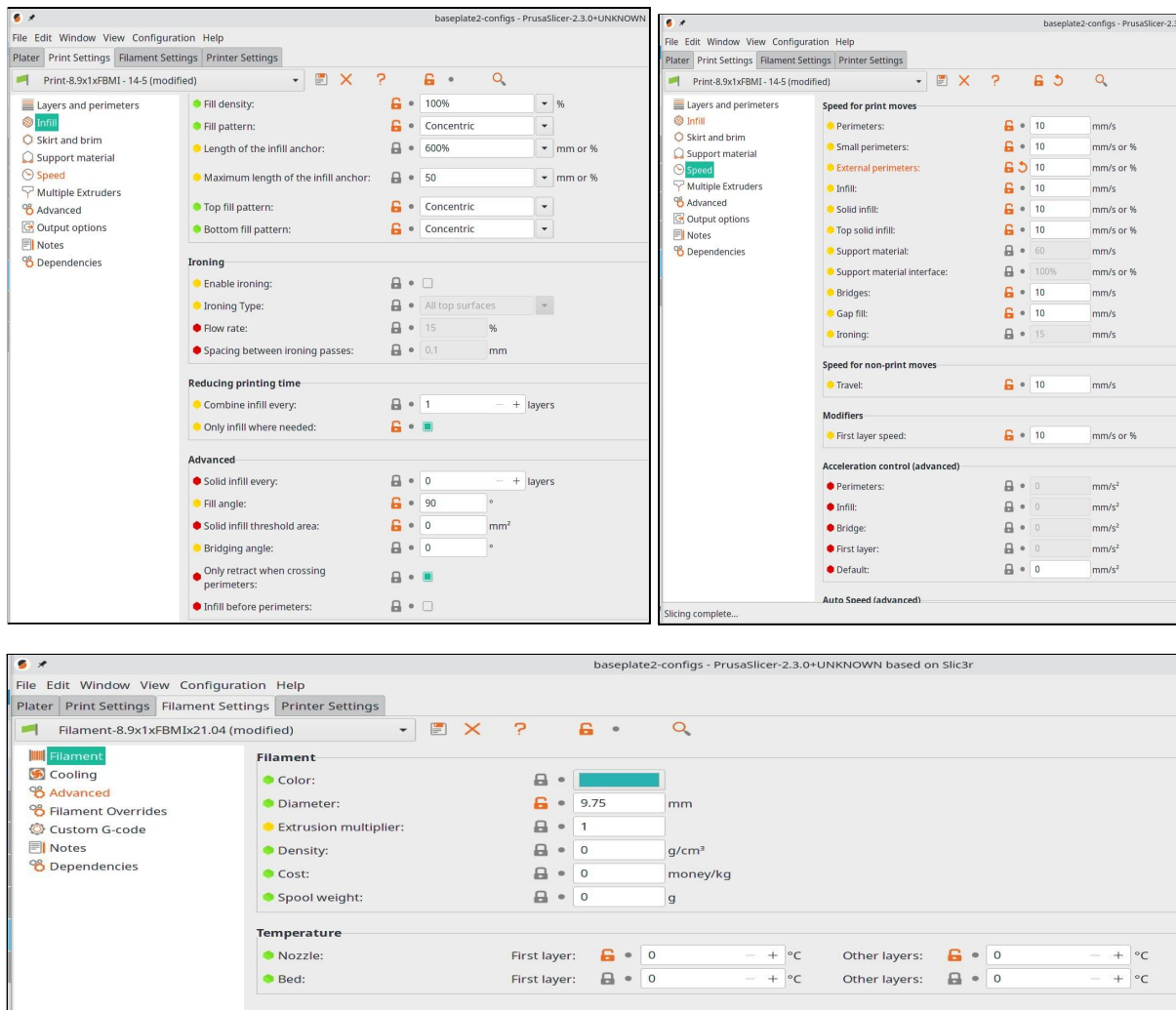


Figure.2.12. changes made during optimization of software.

2.3. Verification of design and printing configurations

1. The fabricated version of the B2V1 design was machined and prepared for printing test constructs on it.
2. Square glass pieces of 25x25 mm dimensions were fixed in place of Nanofiber sheets for testing.
3. The G-code for Circle and Square was inserted into the Repetier-host system and oriented.

4. The Printer was run at first without the extruder needle to see if it followed the path intended.
5. When the printer tried to print the constructs, the changes in motor speed with a different activity caused the printer to misbehave; hence all the speeds needed to be constant.
6. The shape of the extruded test constructs was studied and found to be disfigured. The first extrusion of the bioprinter was extruding too much material causing a bulge to one side.

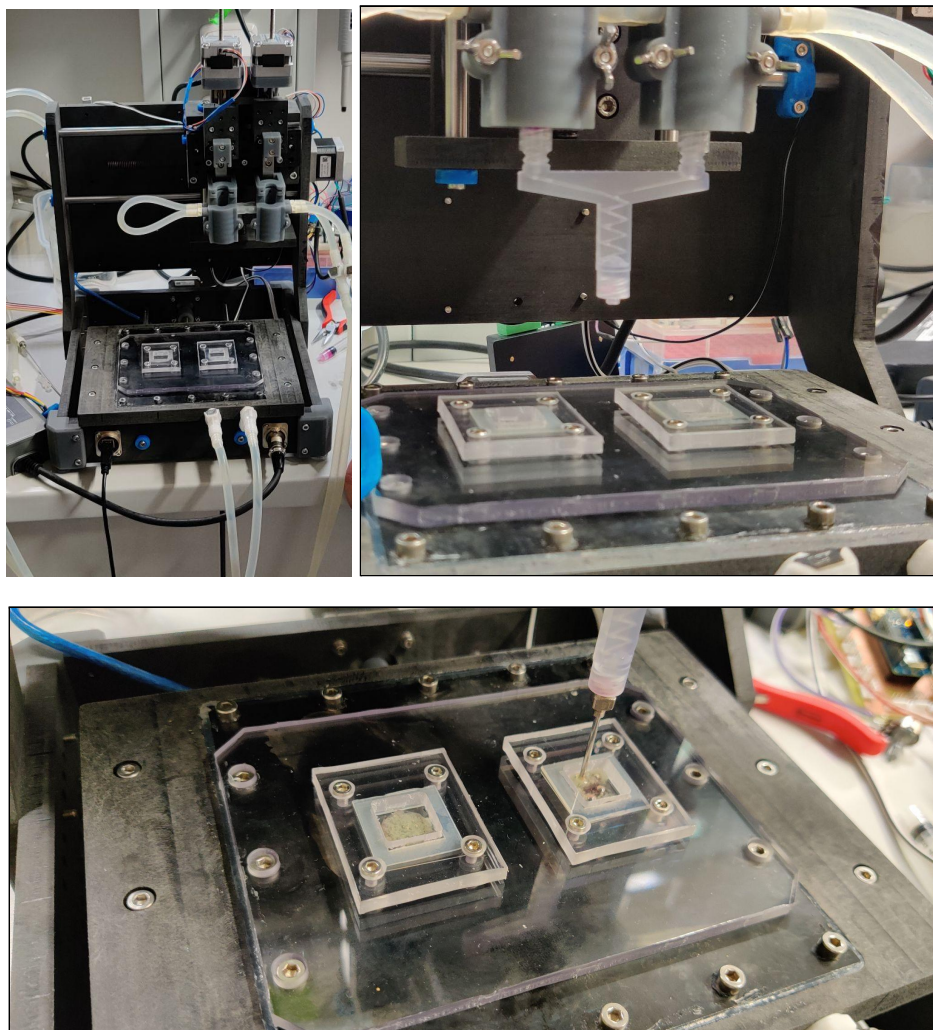


Figure.2.13. Verification of B2V1 fixture design

2.4. Python script prepared to generate G-code

The following Python script was created to create the G-code for a square of adjustable size and position.

```
import math
import json

def generate_gcode(glist):
    print("initializing Gcode file...")
    f = open("square.gcode", "a")
    f.writelines(
        ["\nM42 P5 S1;", "\nM302 S1;", "\nG92 E0;", "\nG1 Z10",
        "F600;", "\nG92 E0;", "\nG21 ; set units to millimeters",
        "\nG90 ; use absolute coordinates", "\nG1 X",
        str(glist[0][0]), " Y", str(glist[0][1]), ";"])
    f.close()
    f = open("square.gcode", "a+")
    print("adding square Gcode")
    for c in glist:
        if glist.index(c)==0:
            f.writelines(["\nG1", " Z", str(0.5), " F400",
            ";", "\nG1", " X", str(c[0]), " Y", str(c[1]), " E",
            str(c[2])])
        else:
            f.writelines(["\nG1", " X", str(c[0]), " Y",
            str(c[1]), " E", str(c[2]), ";"])
    f.close()
```

```

f = open("square.gcode", "a+")

f.writelines(["\nG1 Z27 F600;", "\nG1 X136 Y116 F600; Get
extruder out of the way. Uncomment to use!", "\nM42 P5 S0;",
"\nG91 ; Relative positioning",

            "\nG90 ; Absolute positioning", "\nG92 E0 ;
Reset extruder position", "\nM84 ; Turn steppers off"])

f.close()

print("end gcode")

return f

def extrusion(gcode_list, nozzle_diameter, sirynge_dia):

    TEV = 00.001

    for c in gcode_list:

        if gcode_list.index(c) == 0:

            c.append(TEV)

            x1= c[0]

            y1= c[1]

            continue

        else:

            x2 = c[0]

            y2 = c[1]

            dist = math.sqrt(((x2 - x1) ** 2) + ((y2 - y1) **
2))

            if dist<= nozzle_diameter:

                c.append(TEV)

                x1 = c[0]

```

```

        y1 = c[1]
    elif dist > nozzle_diameter:
        line_volume = dist * math.pi *
(nozzle_diameter / 2) ** 2
        sv = math.pi * (syringe_dia / 2) ** 2
        E_volume = float(line_volume / sv)
        TEV = round((TEV + E_volume), 4)
        c.append(TEV)
        x1 = c[0]
        y1 = c[1]
        continue
    return gcode_list

def square(size, nozzle_diameter, position):
    x_start = position[0] - (size/2) +25
    y_start = position[1] - (size/2) -2
    x_end = position[0] + (size/2)+25
    y_end = position[1] + (size/2) -2
    glist = [[x_start, y_start]]
    print(x_start)
    x1 = x_start
    y1 = y_start
    for c in glist:
        x2 = glist[-1][0]
        y2 = glist[-1][1]
        if x2 >= x_end:

```

```
    if y2 == y_start:
        x1 = glist[-2][0]
        y1 = glist[-2][1]
        glist.append([x2, y_end])
        #print("check4")

    if y2 == y_end:
        print("returning coordinates")
        return glist
    continue

elif y2 == y_start:
    #print("check y2", y2)
    #print("check x2", x2)
    #print("check x1", x1)
    if x2 == x_start:
        glist.append([x2, y_end])
        x1 = glist[-2][0]
        y1 = glist[-2][1]
        print("going up")
        print(x1, y1)
        continue
    elif x2 == x1:
        x2 = x2 + nozzle_diameter
        glist.append([x2, y_start])
        x1 = glist[-2][0]
        y1 = glist[-2][1]
```

```

        print("check2")
        continue
    elif x2 != x1:
        glist.append([x2, y_end])
        x1 = glist[-2][0]
        y1 = glist[-2][1]
        #print("check 3")
        continue
#        continue
    elif y2 == y_end:
        if x2 == x1:
            x2 = x2 + nozzle_diameter
            glist.append([x2, y_end])
            x1 = glist[-2][0]
            y1 = glist[-2][1]
            continue
        elif x2 != x1:
            glist.append([x2, y_start])
            x1 = glist[-2][0]
            y1 = glist[-2][1]
            continue
        continue

## INPUTS
side_of_square = float(input("Enter square dimension :"))
nozzle_diameter = float(input("Enter nozzle diameter : "))

```



```
position_of_center = input("Enter the coordinates to place
the square : ")
resolved_position = json.loads(position_of_center)
print(type(resolved_position[0]))
syringe_diameter = float(input("Enter the diameter of the
syringe : "))

## FUNCTION CALLS
G_coordiinates = square(side_of_square, nozzle_diameter,
resolved_position)
print(G_coordiinates)
extrusion_coordinates = extrusion(G_coordiinates,
nozzle_diameter, syringe_diameter)
print(extrusion_coordinates)
gcode = generate_gcode(extrusion_coordinates)
```

- During the implementation of the G-code, refinements had to be made to orient the printing to the wells of the fixture.
- The Z offset had to be adjusted to allow adherence of the biomaterial to the printer's base.

2.5. Printing on nanofiber substrate

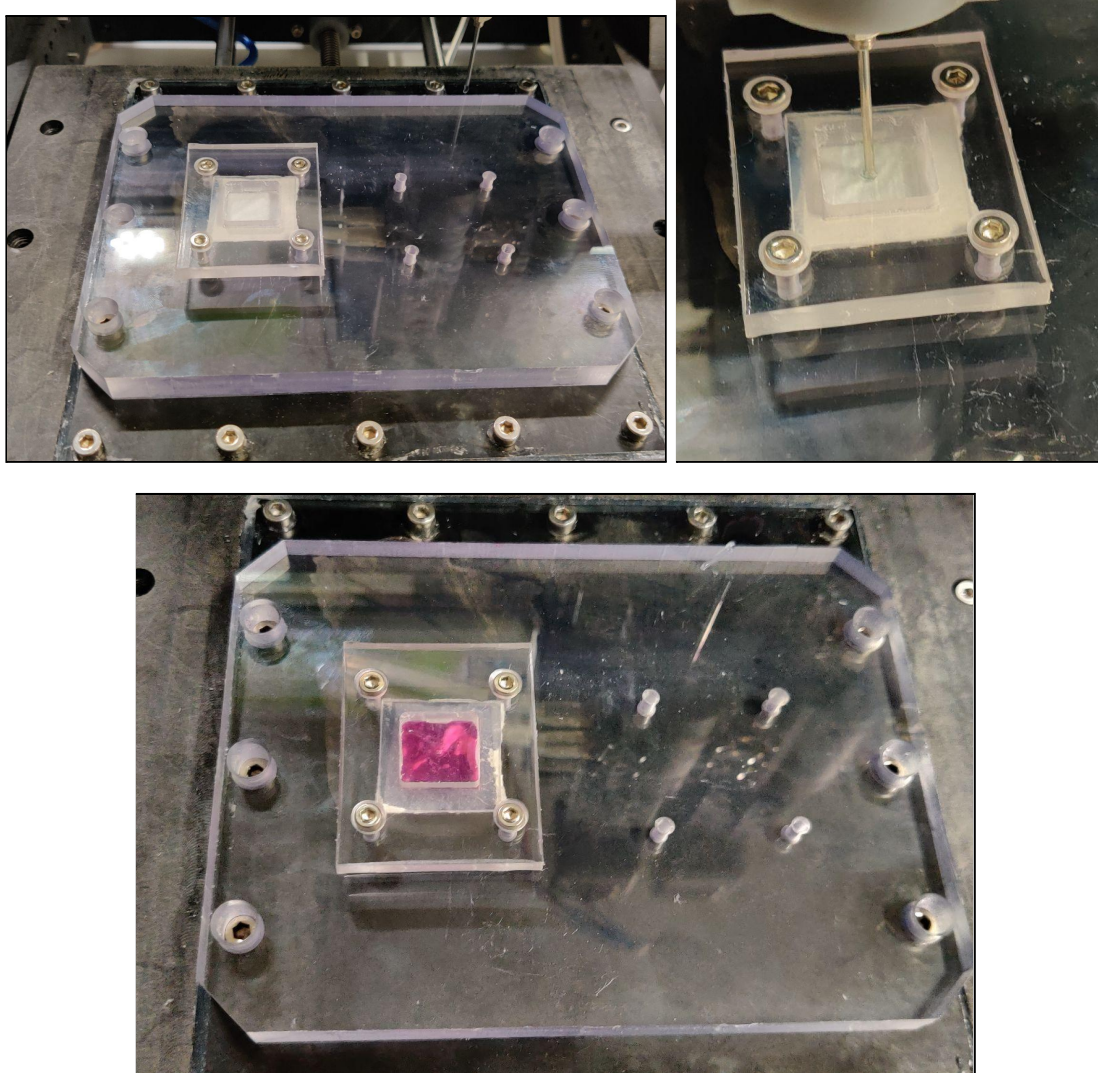


Figure.2.14. The printed construct on nanofiber substrate submerged in culture medium.

- On completing the optimization of the python script to print with the B2V2 design fixture, we printed on Collagen/PCL nanofibers.
- The fibers were fixed under the gasket and clip to create the well.
- A mixture of collagen and porcine stem cells consisted of the bioink being printed on the constructs.
- Culture medium was added to the bio-printed constructs.

2.6. Image analysis and cell counting

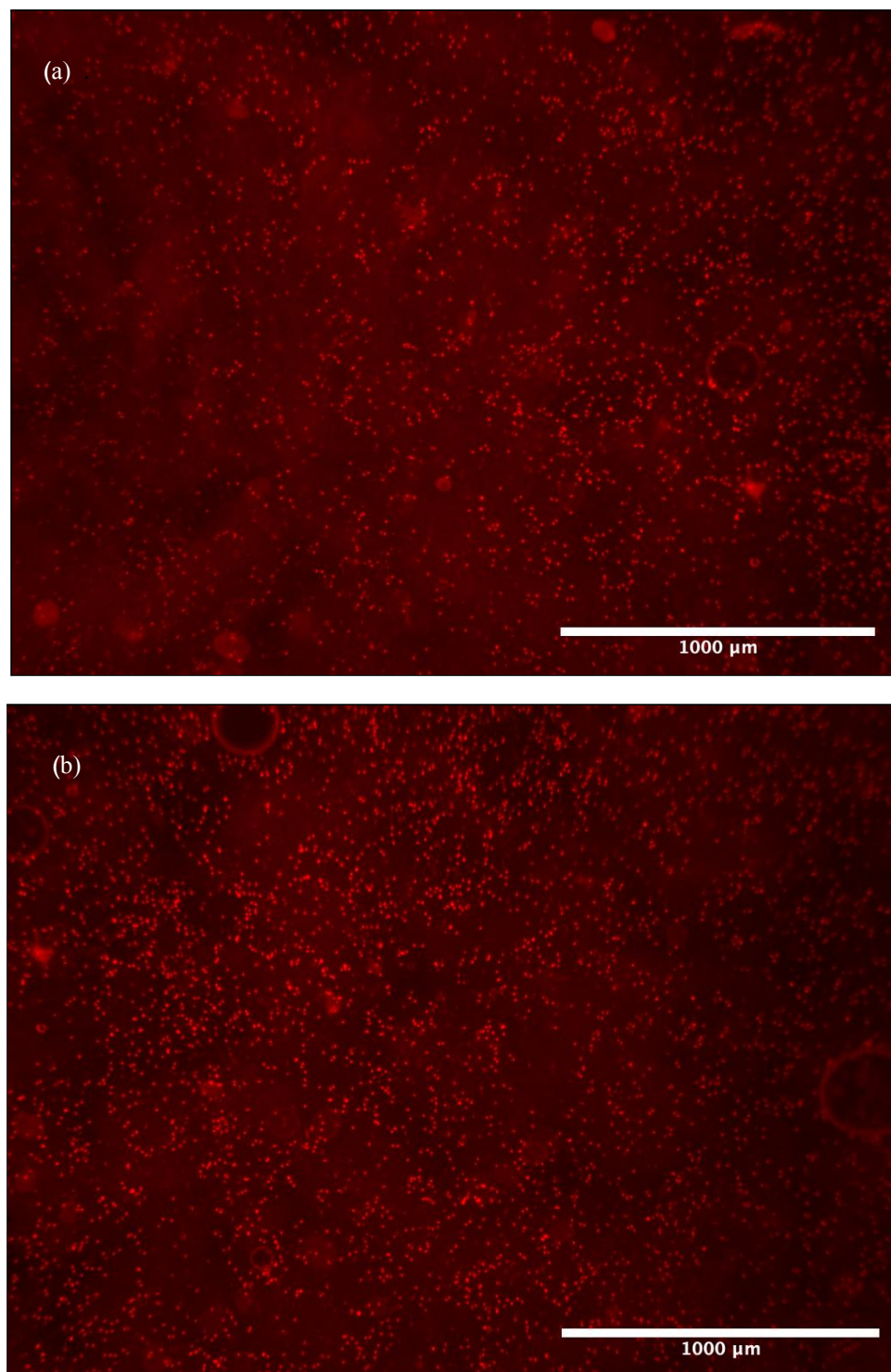


Figure.2.15. Images showing nuclei of porcine stem cells, taken from a fluorescence microscope (a) Print1 (b) Print2.

My thesis supervisor, Ing Roman Matejka, Ph.D., provided the images of cells in a construct. They were captured via a fluorescence microscope half an hour after the printing process.

Image processing to isolate the cells using MATLAB

For the purposes of this code, we assume that the Maximas are the cell nucleus. On measuring the length of the scale on the images, I was also able to verify that the image contains 0.365 pixels per μm .

The algorithm implemented for the purposes of isolating them is shown as the following.

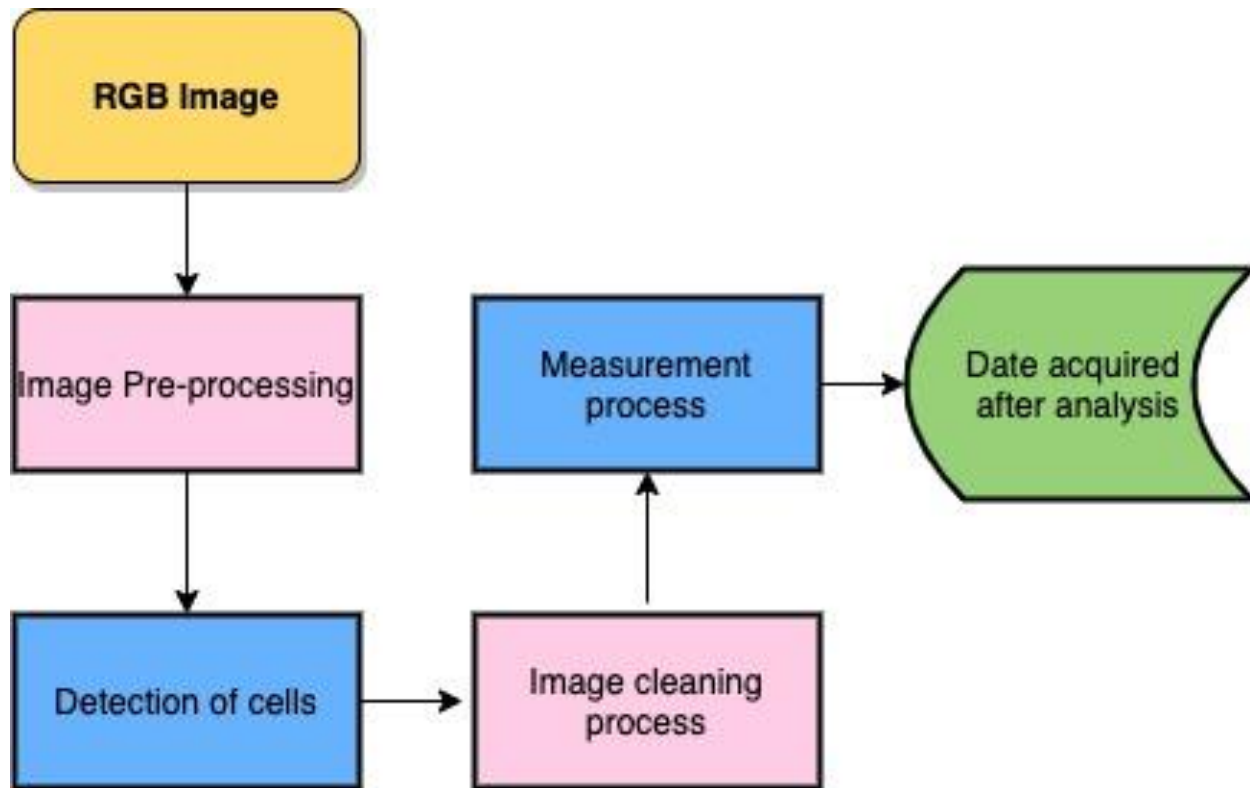


Figure.2.17. The algorithm implemented for cell detection

- The RGB image is used and put through the **pre-processing block**. This segment consisted of cropping the image to remove the measurement scale and text from the picture, isolating the red channel from the RGB image matrix, and then adjusting the image's contrast for better edge detection.
- The main image processing block here is termed "**Detections of the cells,**" which detects cell nuclei through edge detection. We process the edge profiles using Canny, Prewitt, Roberts, LoG, and approxcanny filter and then superimpose the images on each other. This is followed by filling in the holes in the binary image.
- The **image cleaning process** contains the code for removing smaller and larger objects in the binary image and accentuates the cells.
- In the final **measurement process**, the centroids of the cells are mapped, and their radius is calculated; and using the known values of $0.365\text{pxl}/\mu\text{m}$, we can obtain the values in micrometers.

The following is the Matlab code implemented based on the image processing algorithm.

```

clear all
close all

original_image = imread('print2_DAPI.jpg');

%% Pre-processing

[cropped_image,rect] = imcrop(original_image,[0 0 1011 680]);
redChannel = cropped_image(:, :, 1); % isolate red channel
redChannel_contrast_adjust = adapthisteq(redChannel); % contrast adjustment

%% Processing edge detection

[canny_img, thresh_canny] = edge(redChannel_contrast_adjust,'canny');
[prewitt_img, thresh_prewitt] = edge(redChannel_contrast_adjust,'prewitt');
[roberts_img, thresh_roberts] = edge(redChannel_contrast_adjust,'roberts');
[log_img, thresh_log] = edge(redChannel_contrast_adjust,'log');
[approx_canny_img, thresh_approx_canny] = edge(redChannel_contrast_adjust,'approx_canny');
sum_image = double(canny_img)+ double(prewitt_img)+ double(roberts_img)+ double(log_img)+
double(approx_canny_img);
meanImage = sum_image/5;
bin_mean_img = meanImage;
bin_mean_img(bin_mean_img> 0) = 1;
fill_holes = imfill(bin_mean_img,'holes'); % fill holes

%% Cleaning process

pixel_removed = bwareaopen(fill_holes, 2);% remove smaller pixels
dilute_image = imopen(pixel_removed, strel('disk',2)) % Dilute the image
measurements = regionprops(dilute_image, 'Area', 'Perimeter');
large_pixels_removed = bwpropfilt(dilute_image,'Area',[0 200]); % set maximum pixels to 150

%% Measurement

% Get centers and radii of the circles
stats = regionprops('table',large_pixels_removed,'Centroid', ...
'MajorAxisLength','MinorAxisLength');
centers = stats.Centroid;
diameters = mean([stats.MajorAxisLength stats.MinorAxisLength],2);
radii = diameters/2;

% radii in the micrometer

radii_micrometer = radii/0.365;
Average_radii_micro = mean(radii_micrometer);
minimum_rarius_micro = min(radii_micrometer);
maximum_radius = max(radii_micrometer);
standard_deviation = std(radii_micrometer);

```

```
%% Probability
```

```
probability_measurements = regionprops(large_pixels_removed, 'Area', 'Perimeter');
```

```
all_area_list = [probability_measurements.Area];
```

```
total_area_cells = sum(all_area_list);
```

```
[m,n] = size(large_pixels_removed);
```

```
area_of_image = m*n;
```

```
probability_finding_cell = total_area_cells/area_of_image;
```

3. Results

3.1 Verification of design

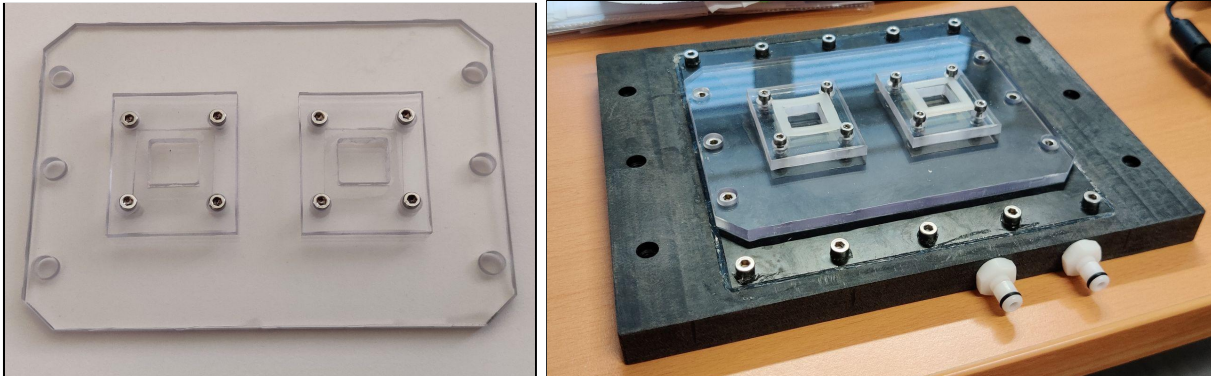
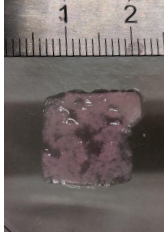

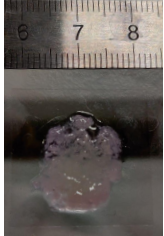
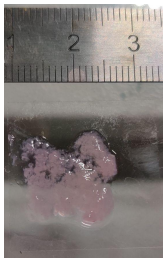
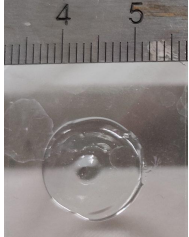
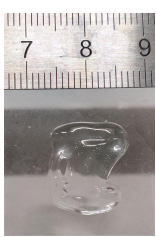


Figure.3.1. Picture of B2V1 fixture machined

The Polycarbonate fixture is shown in figure.3.1 is based on B2V1. It sits on the lower bed fixture that settles onto the custom 3D-biprinter, as shown in Fig. 3.1b.

Table 3.1 Results of the verification process.

Constructs	Desired dimension	Observed Dimensions	Pictures
Circle	2 x 13	1.5 x 15 x 16	

Square	2 x 13 x13	1.5 x 16 x 15	 
Circle	1 x 13	1 x 15	
H- shaped	1 x 13 x 13	1 x 16 x 13	
Circle	1 x 13	1 x 13	
H- shaped	1 x 13	1 x 13 x 14	

We observe that the baseplate was getting warped due to screwing and unscrewing of the bolts, causing a difference in the Z direction. This causes the extruder point to get blocked, causing a considerable amount to come out suddenly. The resultant prints are dimensionally comparable but not accurate.

3.2. G-code generated by the Python script.

```

M42 P5 S1;
M302 S1;
G92 E0;
G1 Z10 F600;
G92 E0;
G21 ; set units to millimeters
G90 ; use absolute coordinates
G1 X56.5 Y49.5;
G1 Z0.5 F400;
G1 X56.5 Y49.5 E0.001
G1 X56.5 Y62.5 E0.1378;
G1 X57.5 Y62.5 E0.1378;
G1 X57.5 Y49.5 E0.2746;
G1 X58.5 Y49.5 E0.2746;
G1 X58.5 Y62.5 E0.4114;
G1 X59.5 Y62.5 E0.4114;
G1 X59.5 Y49.5 E0.5482;
G1 X60.5 Y49.5 E0.5482;
G1 X60.5 Y62.5 E0.685;
G1 X61.5 Y62.5 E0.685;
G1 X61.5 Y49.5 E0.8218;
G1 X62.5 Y49.5 E0.8218;
G1 X62.5 Y62.5 E0.9586;
G1 X63.5 Y62.5 E0.9586;
G1 X63.5 Y49.5 E1.0954;
G1 X64.5 Y49.5 E1.0954;
G1 X64.5 Y62.5 E1.2322;
G1 X65.5 Y62.5 E1.2322;
G1 X65.5 Y49.5 E1.369;
G1 X66.5 Y49.5 E1.369;
G1 X66.5 Y62.5 E1.5058;
G1 X67.5 Y62.5 E1.5058;
G1 X67.5 Y49.5 E1.6426;
G1 X68.5 Y49.5 E1.6426;
G1 X68.5 Y62.5 E1.7794;
G1 X69.5 Y62.5 E1.7794;
G1 Z27 F600;
G1 X136 Y116 F600; Get extruder out of the way. Uncomment to use!
M42 P5 S0;
G91; Relative positioning
G90; Absolute positioning
G92 E0 ; Reset extruder position
M84; Turn steppers off

```

Over a G-code visualizer, the generated code is following the intended path, however, when the code is uploaded to the bioprinter. The plunger was pushed down incredibly fast.

Once the alterations were made to the code regarding the positioning and offset, a decidedly better outcome was visible, as you can see below.

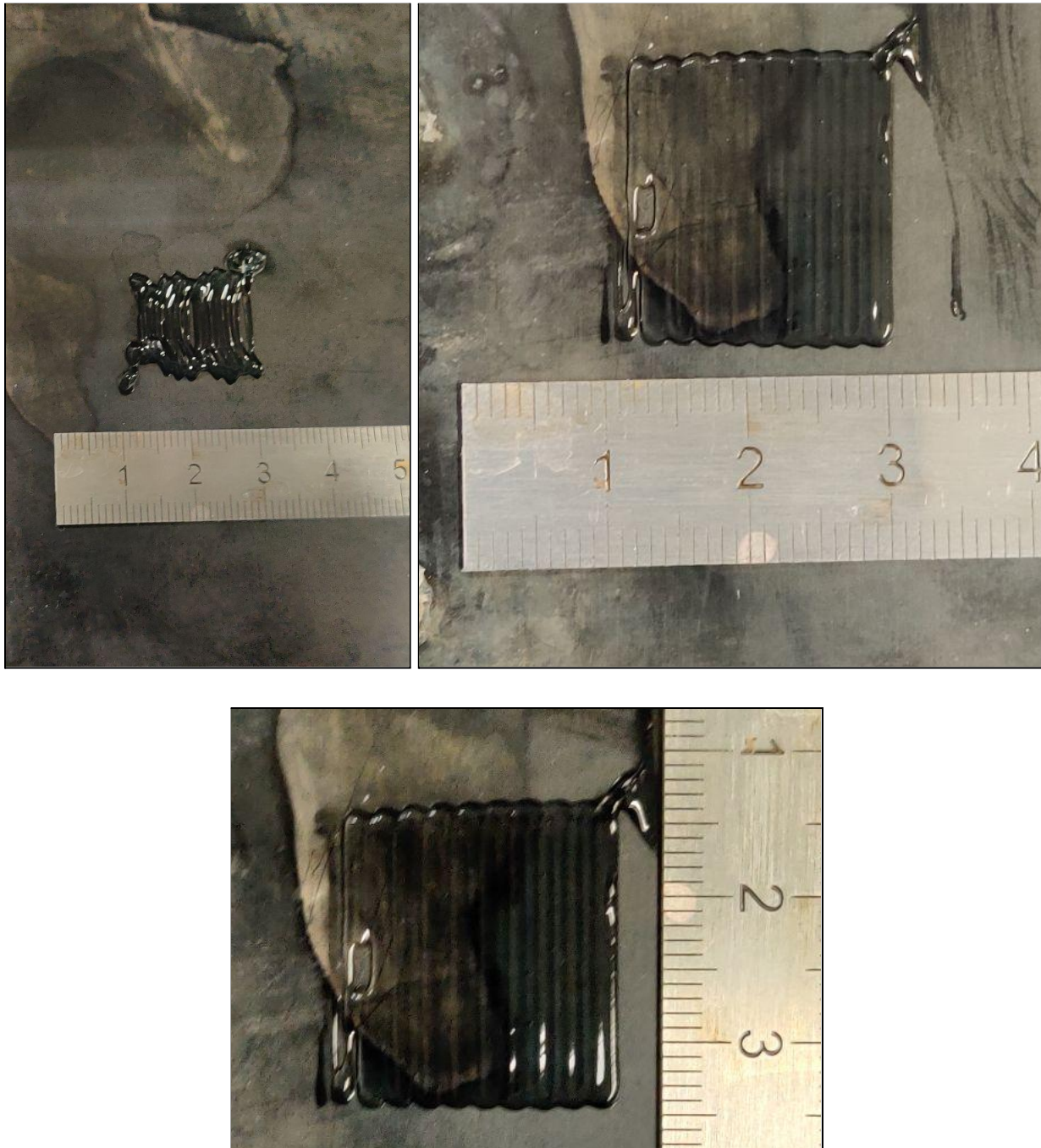


Figure.3.2. They are the constructs printed while optimizing the python code for the bioprinter

3.3. Image analysis and cell counting

Table.3.2. Results from the processing code for Print1

Print1	
Number of cells detected	1818
Maximum cell radius (μm)	30.4337
Minimum cell radius (μm)	5.9022
Average cell radius (μm)	10.6573
Standard Deviation in radius (μm)	3.2826

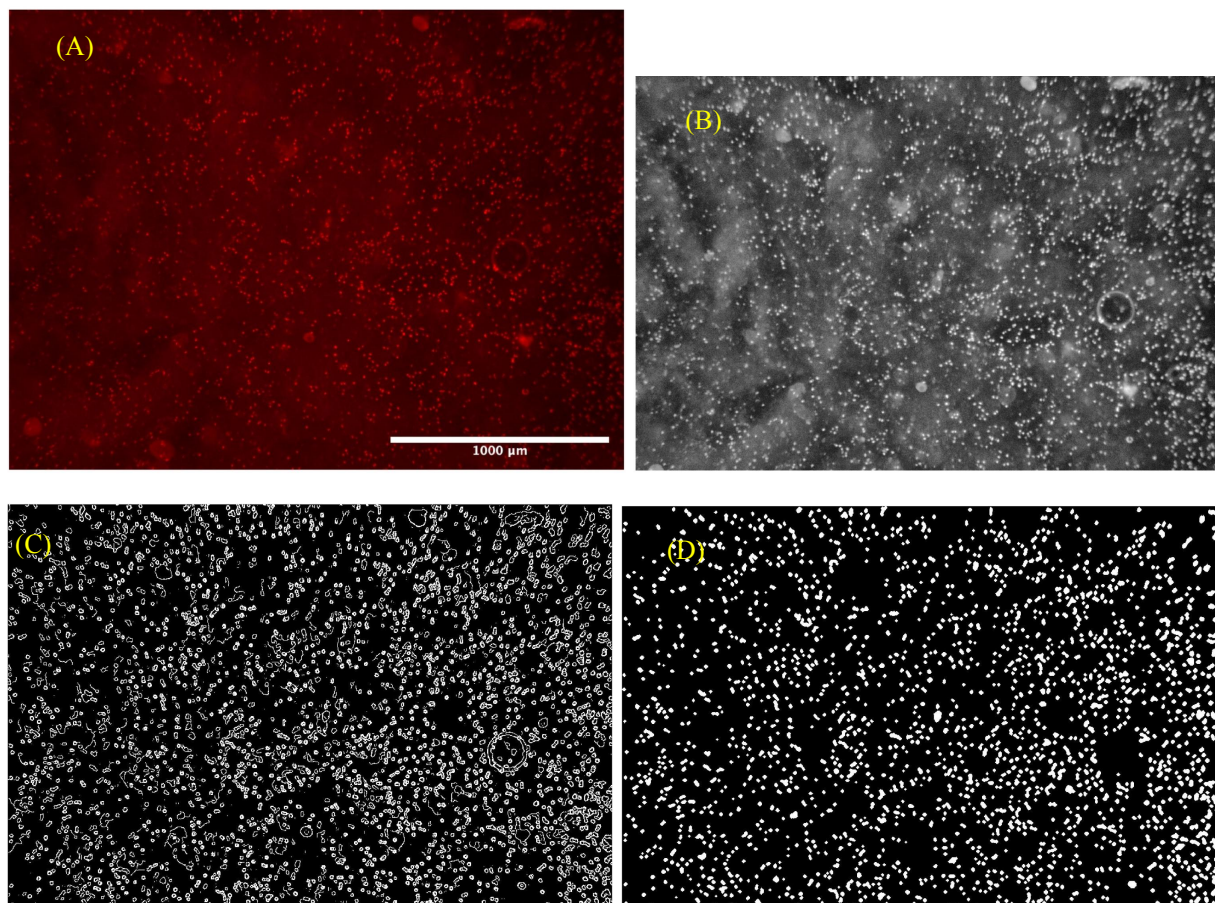


Figure.3.3. Print1 : (A) Original RGB image, (B) Red channel isolated and contrast adjusted, (C) Image sum of edge detection filters output, (D) Holed filled and the image cleaned for measurements.

Table.3.2. Results from the processing code for Print2

Print2	
Number of cells detected	2057
Maximum cell radius (μm)	29.2783
Minimum cell radius (μm)	5.9022
Average cell radius (μm)	10.9289
Standard Deviation in radius (μm)	3.6830

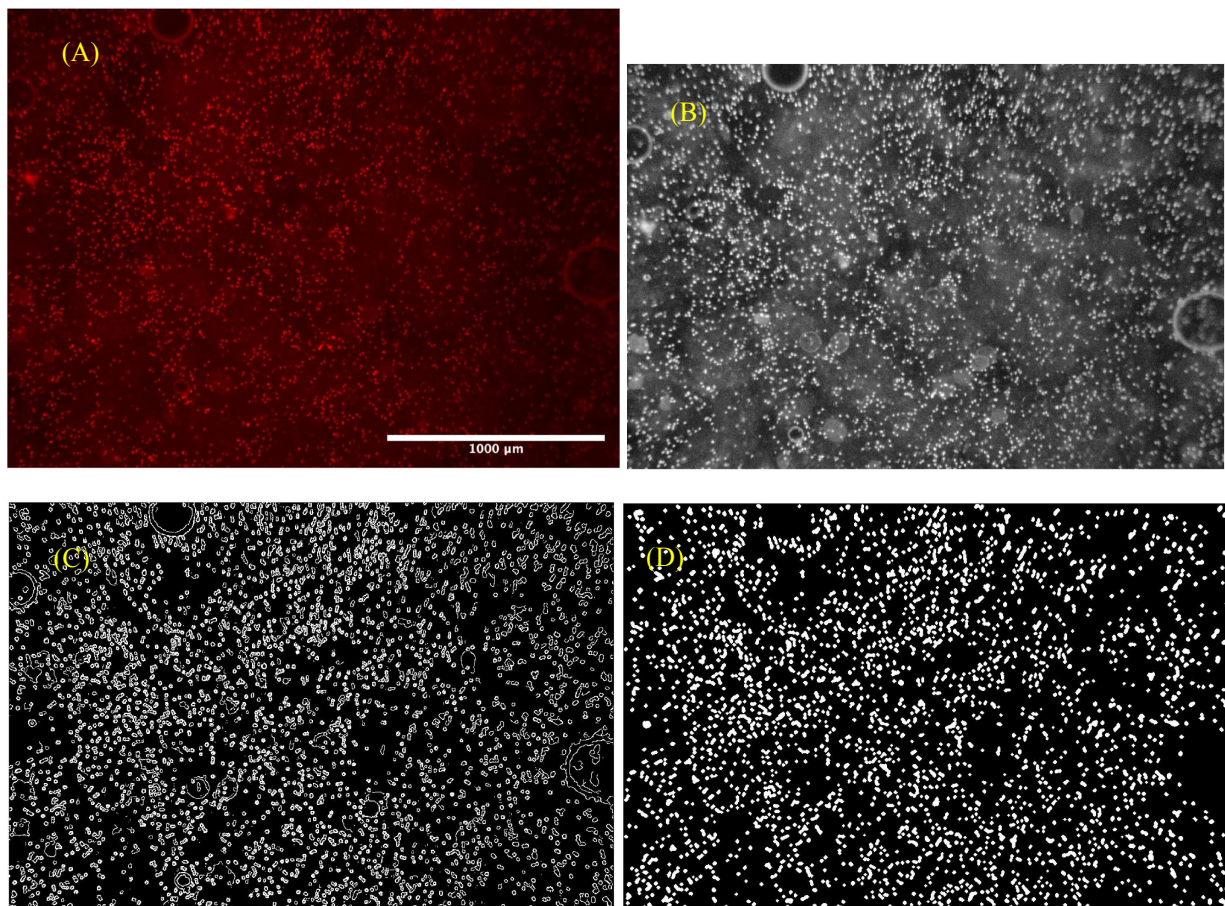


Figure.3.4. Print2 : (A) Original RGB image, (B) Red channel isolated and contrast adjusted, (C) Image sum of edge detection filters output, (D) Holed filled and the image cleaned for measurements.

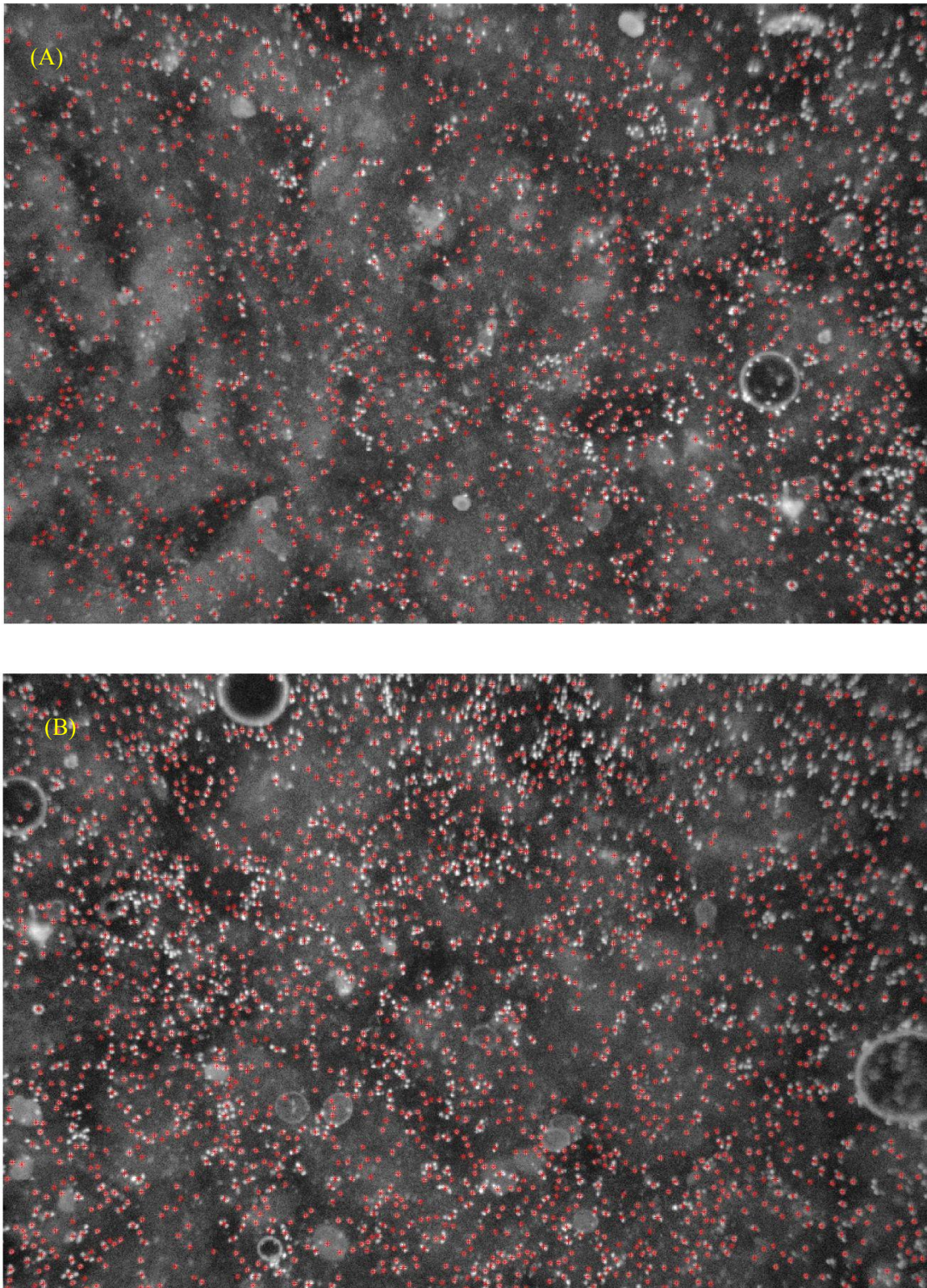


Figure.3.5.(A) Centroids mapped on the Grayscale images of Print1 and (B)Centroids mapped on the Grayscale images of Print2.

4. Discussion

4.1. Verification of the design and configurations

While printing the test prints on glass coverslips, we found that the extruder tool was spurting out the bioink at some points in the pattern.

After calibrating the needle on the Z-axis, it still showed the same error while printing. The printing was stopped once the extruder tool started to bend. This effect was because of the warping of the mounting fixture's base, due to the thickness of 5mm and the screws pulling in the polycarbonate slab.

The results of the verification process show an extra amount of bio-ink being extruded at every layer. This can be attributed to the G-code where 1.2 times the extrusion is being generated.

4.2. Python script for G-code

With the output of the script, we could realize that the error was due to a large number of decimal places for the extruder values. The float values were rounded to four decimal places, and a new G-code file was generated. You can see this in Figure 3.2. The alignment of the printed lines became straighter, so they better stick to each other. Successive refinements to the code lead to the extrusion path working optimally, allowing us to commence printing on nanofiber substrate.

4.3. Image analysis and cell counting

The fluorescence in the images is due to the DAPI(4',6-diamidino-2-phenylindole) counterstain that binds to the DNA or RNA; you can only observe the nuclei of the cells. Because of its high affinity for DNA, it is frequently used for cell counting, cell sorting based on DNA content, and nuclear segmentation. The cores are distributed over the entire construct, as visible in the images of Figure.3.7. Whether or not the bioink can adequately distribute the stem cells in the 3D printed constructs is an essential characteristic of bio-inks and the printing strategy.

Edge detection is a set of mathematical methods that aim to identify points in an image with sudden changes in pixel values. The points in which image brightness changes sharply and organize into curved line segments. Edge detection is one of the fundamental steps in image processing, image analysis, and pattern recognition.

One of the most potent edge detection methods the “edge()” command provides is the **Canny** method. The canny method differs from other edge detection methods as it uses two different threshold levels to detect strong and weak edges. It then includes the weak edges in the output only if they are connected to the strong edges. The algorithm contains the following steps.

1. Convolution with Gaussian Filter Coefficient
2. Convolution with Canny Filter for Horizontal and Vertical orientation
3. Calculating directions using atan2
4. Adjusting to nearest 0, 45, 90, and 135 degree
5. Non-Maximum Suppression
6. Hysteresis Thresholding

The **Prewitt** operator detects two types of edges, horizontal and vertical edges. The edges are calculated by using the difference between the corresponding pixel intensities of an image. Changes in a digital image can only be calculated using differentiation; that is why all the masks used for edge detection can also be known as derivative masks. The Prewitt operator

provides us with two masks, one for the detection of edges in the vertical direction and one in the horizontal direction.

Mask for the vertical direction

-1	0	1
-1	0	1
-1	0	1

When you convolve this mask on an image, it gives you the vertical edges of the image. It simply works as a first-order derivative and calculates the pixel intensities. As the middle column is zeros, it does not give the original values of an image but instead calculates the difference in right and left pixel values. This increases the edge intensities and enhances the values.

Mask for the horizontal direction

-1	-1	-1
0	0	0
1	1	1

Similar to the vertical mask, the Horizontal mask contains a middle row containing zeros. It does not give the original values but calculates the difference of above and below pixel intensities of a particular edge.

The Roberts operator performs a simple 2-D spatial gradient measurement on an image. It thus highlights regions of high spatial frequency which often corresponds to edges. Pixel values at each point in the output represent the estimated absolute magnitude of the spatial gradient of the input image at that point. This operator contains a pair of 2x2 convolution kernels given below, namely, G_x and G_y . One kernel is simply the other rotated by 90° .

G_x

+1	0
0	-1

Gy

0	+1
-1	0

These kernels are designed to respond maximally to edges running at 45° to the pixel grid, one kernel for each of the two perpendicular orientations. The kernels can be applied separately to the input image to produce separate measurements of the gradient component in each direction. These can then be combined to find the absolute magnitude of the gradient at each point and the orientation of that gradient.

The LoG method or the “Laplacian of Gaussian” detects edges by using the double derivative over an image smoothed by a Gaussian filter. Laplacian filters are derivative filters used to find areas with rapid changes in a digital image. As derivative filters are sensitive to noise, it is common to smooth the image with the help of a Gaussian filter before applying the Laplacian filter. This two-step process is known as the LoG method.

The Approxcanny operator Finds edges using an approximate version of the Canny edge detection algorithm that provides faster execution time at the expense of less precise detection. Floating-point images are expected to be normalized to the range [0, 1].

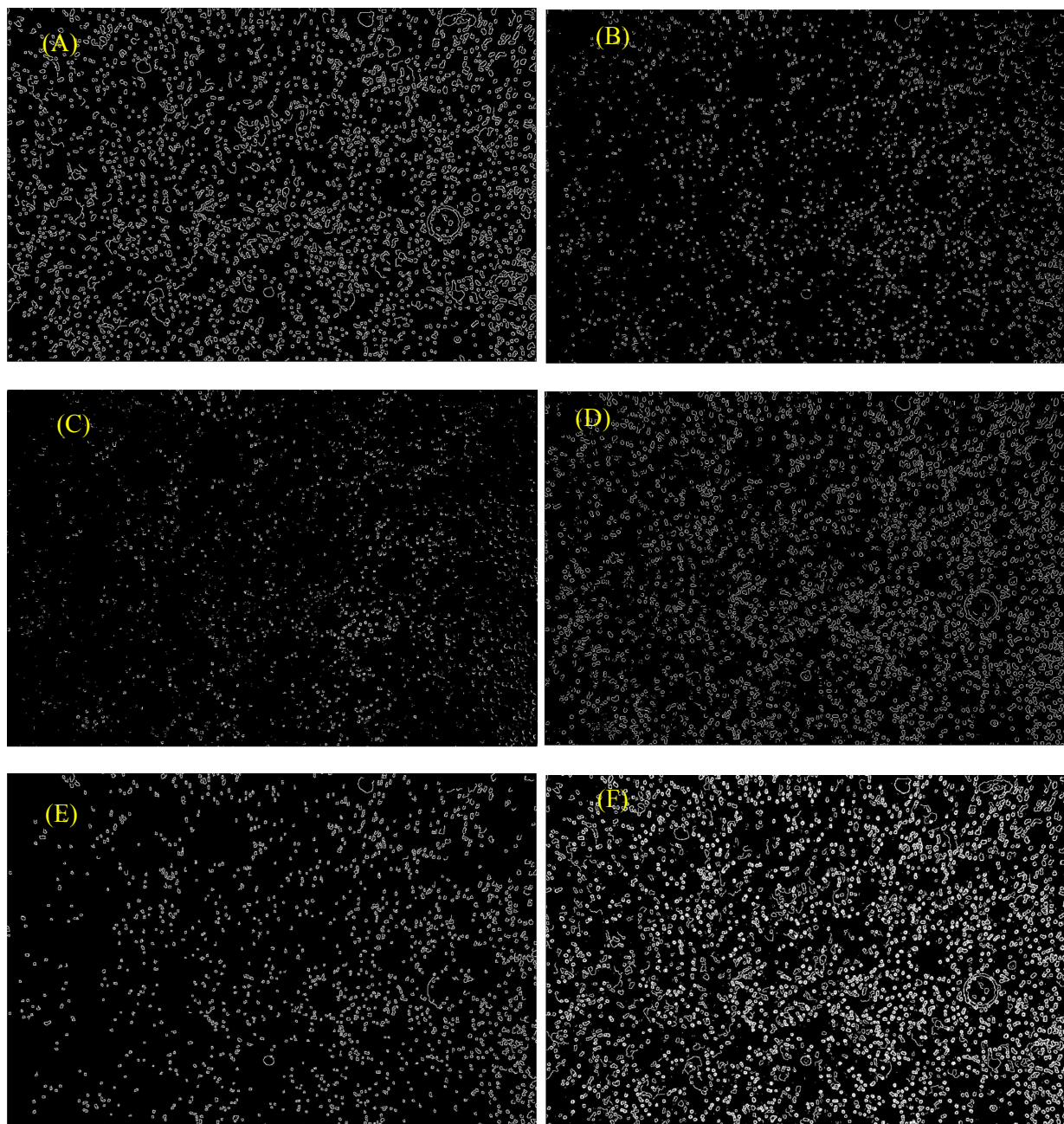


Figure.4.1. (A)The output of Image through Canny method, (B)Output of Image through Prewitt method, (C)Output of Image through Roberts method, (D)Output of Image through LoG method,(E)Output of Image through Approxcanny method, (F) The mean image of all the method outputs and set all values higher than 0 to 1.

Initial trials of edge detection were done using the Canny operator. The output image contains the edges of most of the nuclei, but the edges do not connect back to form circles. Forming closed objects was required for the next step of filling holes. At which point, less than 50 % of the nuclei were being highlighted. So, I tested out the other available operators for edge detection, and the second most effective method was the LoG method. The LoG method

highlighted even some of the edges on the boundary cells. But, none of the outputs individually clearly showed the finished edges. For this reason, I superimposed the images on top of each other to reduce those gaps in the edges, as you can observe in Figure.4.1.(F).

On implementing the processing algorithm, I got the image for the count of cells which I then used to get the centers of the nuclei. I have plotted the centroids on top of the Grayscale images, as you can see in Figure. 3.7. The cells being overlapped by the centroids are visible along with the few that have been eliminated during the cleaning process. The area of these cells has been calculated and used to clean the image further by removing objects being detected that are larger than 200 pixels; this was done to eliminate artifacts of larger size from the image.

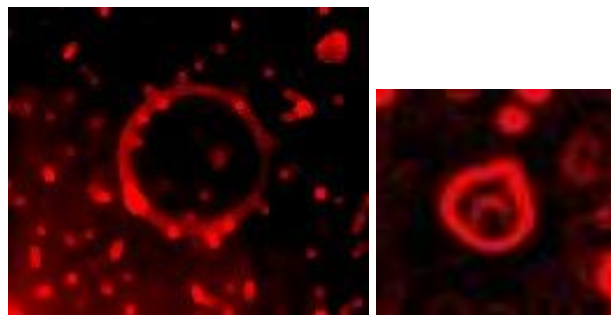


Figure.4.2. Magnified and contrast-enhanced images of bubble artifacts in the printed construct

Observing the magnified portions from the prints you can observe bubbles trapped in the 3D construct with the prominent nuclei around them. The presence of these artifacts causes the ring shape of the bubbles to be picked up in edge erection, causing the code to omit nuclei on the edges of the bubbles. Some cells get excluded in the cleaning process of the algorithm which would work better with varying the thresholds. In some cases, we can also observe that two or more cells that are too close together to be distinguished as two separate entities give a single cell center averaged between them.

The probability of finding a cell at any given location in the images is 12.12 % for Print1 and 14.17 % for Print2. This implies that there is approximately 2.05 % more chance of locating a cell in Print2 than in Print1. The algorithm used for the isolation of the cells is adequate and isolates a majority of the cells, but this can be improved to process a continuous line of images.

5. Conclusions

From the verification procedure, we can conclude that the thickness of the base plate was lesser than required and did not have adequate strength to maintain its structure correctly. A fixture with a thickness of 10mm for the base plate will be sufficient to maintain the structural integrity through successive use of the fixture.

The Optimization of this system depended highly on the G-code formulation and debugging. The G-code generated by Prusa-sliced was causing extra extrusion values causing deformity in the printed constructs. I wrote a python script to take complete control and generate the G-code for squares of any size at the position of our choosing or extruding nozzle of any size. The program additionally accommodates changes in the syringe diameter as well as the extruder diameter. After a few iterations in the code, it was capable of printing over the nanofiber substrates placed in the fixture well.

Image processing and analysis were done on substitute pictures of DAPI counterstain stained prints highlighting the nuclear material of the stem cells. An algorithm was devised and implemented in Matlab using edge detection. I put the images through the code to isolate the cells and get their measurements. These show an adequate distribution of cells through the print. The pASCs of average radius $10.6573 \pm 3.2826 \mu\text{m}$ for Print1 and $10.9289 \pm 3.6830 \mu\text{m}$ for Print2 were detected. The cells appear to be adequately and evenly embedded in the bioink based constructs. The probability of finding a nucleus occupying a particular area on Print1 is 12.12% and 14.17% for Print2.

List of Literature

- [1] D. Sundaramurthi, S. Rauf, and C. A. E. Hauser, “3D bioprinting technology for regenerative medicine applications,” *Int. J. Bioprinting*, vol. 2, no. 2, pp. 9–26, 2016, doi: 10.18063/IJB.2016.02.010.
- [2] M. Vaezi, G. Zhong, H. Kalami, and S. Yang, *Extrusion-based 3D printing technologies for 3D scaffold engineering*. Elsevier Ltd, 2018.
- [3] D. E. Mouzakis, “Advanced Technologies in Manufacturing 3D-Layered Structures for Defense and Aerospace,” *Lamination - Theory Appl.*, 2018, doi: 10.5772/intechopen.74331.
- [4] A. Saxena and M. Kamran, “A Comprehensive Study on 3D Printing Technology,” *MIT Int. J. Mech. Eng.*, vol. 6, no. 2, pp. 63–69, 2016, [Online]. Available: <https://www.researchgate.net/publication/310961474>.
- [5] C. F. Barker and J. F. Markmann, “Historical overview of transplantation,” *Cold Spring Harb. Perspect. Med.*, vol. 3, no. 4, 2013, doi: 10.1101/cshperspect.a014977.
- [6] A. B. Dababneh and I. T. Ozbolat, “Bioprinting Technology: A Current State-of-the-Art Review,” *J. Manuf. Sci. Eng. Trans. ASME*, vol. 136, no. 6, pp. 1–11, 2014, doi: 10.1115/1.4028512.
- [7] T. H. Jovic, E. J. Combella, Z. M. Jessop, and I. S. Whitaker, “3D Bioprinting and the Future of Surgery,” *Front. Surg.*, vol. 7, no. November, pp. 1–10, 2020, doi: 10.3389/fsurg.2020.609836.

- [8] B. Duan, “State-of-the-Art Review of 3D Bioprinting for Cardiovascular Tissue Engineering,” *Ann. Biomed. Eng.*, vol. 45, no. 1, pp. 195–209, 2017, doi: 10.1007/s10439-016-1607-5.
- [9] A. Atala, “Tissue engineering of human bladder,” *Br. Med. Bull.*, vol. 97, no. 1, pp. 81–104, 2011, doi: 10.1093/bmb/ldr003.
- [10] P. R. Corridon, I. K. Ko, J. J. Yoo, and A. Atala, “Bioartificial Kidneys,” *Curr. Stem Cell Reports*, vol. 3, no. 2, pp. 68–76, 2017, doi: 10.1007/s40778-017-0079-3.
- [11] S. V. Murphy and A. Atala, “3D bioprinting of tissues and organs,” *Nat. Biotechnol.*, vol. 32, no. 8, pp. 773–785, 2014, doi: 10.1038/nbt.2958.
- [12] S. Naghieh and D. Chen, “Printability – a Key Issue in Extrusion-based Bioprinting,” *J. Pharm. Anal.*, 2021, doi: 10.1016/j.jpha.2021.02.001.
- [13] P. Studies, “Bioprinting and characterization of medium viscosity alginate scaffold for nerve tissue regeneration,” no. August, 2019.
- [14] H. Lee, G. H. Yang, M. Kim, J. Y. Lee, J. T. Huh, and G. H. Kim, “Fabrication of micro/nanoporous collagen/dECM/silk-fibroin biocomposite scaffolds using a low temperature 3D printing process for bone tissue regeneration,” *Mater. Sci. Eng. C*, vol. 84, no. September 2017, pp. 140–147, 2018, doi: 10.1016/j.msec.2017.11.013.
- [15] E. Koçak, A. Yıldız, and F. Acartürk, “Three dimensional bioprinting technology: Applications in pharmaceutical and biomedical area,” *Colloids Surfaces B Biointerfaces*, vol. 197, 2021, doi: 10.1016/j.colsurfb.2020.111396.

- [16] S. V. Murphy, A. Skardal, and A. Atala, "Evaluation of hydrogels for bio-printing applications," *J. Biomed. Mater. Res. - Part A*, vol. 101 A, no. 1, pp. 272–284, 2013, doi: 10.1002/jbm.a.34326.
- [17] I. T. Ozbolat and M. Hospodiuk, "Current advances and future perspectives in extrusion-based bioprinting," *Biomaterials*, vol. 76, pp. 321–343, 2016, doi: 10.1016/j.biomaterials.2015.10.076.
- [18] D. Kang *et al.*, "Pre-set extrusion bioprinting for multiscale heterogeneous tissue structure fabrication," *Biofabrication*, vol. 10, no. 3, 2018, doi: 10.1088/1758-5090/aac70b.
- [19] S. Agarwala, "A perspective on 3D bioprinting technology: Present and future," *Am. J. Eng. Appl. Sci.*, vol. 9, no. 4, pp. 985–990, 2016, doi: 10.3844/ajeassp.2016.985.990.
- [20] D. F. Duarte Campos *et al.*, "Corneal bioprinting utilizing collagen-based bioinks and primary human keratocytes," *J. Biomed. Mater. Res. - Part A*, vol. 107, no. 9, pp. 1945–1953, 2019, doi: 10.1002/jbm.a.36702.
- [21] S. Iwanaga, K. Arai, and M. Nakamura, *Inkjet bioprinting*. Elsevier Inc., 2015.
- [22] D. J. Odde and M. J. Renn, "Laser-guided direct writing for applications in biotechnology," *Trends Biotechnol.*, vol. 17, no. 10, pp. 385–389, 1999, doi: 10.1016/S0167-7799(99)01355-4.
- [23] S. Michael *et al.*, "Tissue Engineered Skin Substitutes Created by Laser-Assisted Bioprinting Form Skin-Like Structures in the Dorsal Skin Fold Chamber in Mice," *PLoS One*, vol. 8, no. 3, 2013, doi: 10.1371/journal.pone.0057741.

- [24] S. Michael *et al.*, “Tissue Engineered Skin Substitutes Created by Laser-Assisted Bioprinting Form Skin-Like Structures in the Dorsal Skin Fold Chamber in Mice,” *PLoS One*, vol. 8, no. 3, 2013, doi: 10.1371/journal.pone.0057741.
- [25] B. Guillotin *et al.*, “Laser assisted bioprinting of engineered tissue with high cell density and microscale organization,” *Biomaterials*, vol. 31, no. 28, pp. 7250–7256, 2010, doi: 10.1016/j.biomaterials.2010.05.055.
- [26] S. Loai, B. R. Kingston, Z. Wang, and D. N. Philpott, “Clinical Perspectives on 3D Bioprinting Paradigms for Regenerative Medicine,” *Regen. Med. Front.*, pp. 1–40, 2019, doi: 10.20900/rmf20190004.
- [27] R. Raman and R. Bashir, *Stereolithographic 3D bioprinting for biomedical applications*. Elsevier Inc., 2015.
- [28] J. Stampfl *et al.*, “Photopolymers with tunable mechanical properties processed by laser-based high-resolution stereolithography,” *J. Micromechanics Microengineering*, vol. 18, no. 12, 2008, doi: 10.1088/0960-1317/18/12/125014.
- [29] K. E. Drzewiecki, J. N. Malavade, I. Ahmed, C. J. Lowe, and D. I. Shreiber, “A thermoreversible, photocrosslinkable collagen bio-ink for free-form fabrication of scaffolds for regenerative medicine,” *Technology*, vol. 05, no. 04, pp. 185–195, 2017, doi: 10.1142/s2339547817500091.
- [30] Ž. P. Kačarević *et al.*, “An introduction to 3D bioprinting: Possibilities, challenges and future aspects,” *Materials (Basel)*, vol. 11, no. 11, 2018, doi: 10.3390/ma11112199.
- [31] D. E. Mouzakis, “Advanced Technologies in Manufacturing 3D-Layered Structures for Defense and Aerospace,” *Lamination - Theory Appl.*, 2018, doi: 10.5772/intechopen.74331.

- [32] J. Ma, Y. Wang, and J. Liu, “Bioprinting of 3D tissues/organs combined with microfluidics,” *RSC Adv.*, vol. 8, no. 39, pp. 21712–21727, 2018, doi: 10.1039/c8ra03022g.
- [33] I. T. Ozbolat and M. Hospodiuk, “Current advances and future perspectives in extrusion-based bioprinting,” *Biomaterials*, vol. 76, pp. 321–343, 2016, doi: 10.1016/j.biomaterials.2015.10.076.
- [34] M. Vaezi, G. Zhong, H. Kalami, and S. Yang, *Extrusion-based 3D printing technologies for 3D scaffold engineering*. Elsevier Ltd, 2018.
- [35] Y. B. Kim, H. Lee, and G. H. Kim, “Strategy to Achieve Highly Porous/Biocompatible Macroscale Cell Blocks, Using a Collagen/Genipin-bioink and an Optimal 3D Printing Process,” *ACS Appl. Mater. Interfaces*, vol. 8, no. 47, pp. 32230–32240, 2016, doi: 10.1021/acsami.6b11669.
- [36] I. T. Ozbolat and M. Hospodiuk, “Current advances and future perspectives in extrusion-based bioprinting,” *Biomaterials*, vol. 76, pp. 321–343, 2016, doi: 10.1016/j.biomaterials.2015.10.076.
- [37] A. Mazzocchi, M. Devarasetty, R. Huntwork, S. Soker, and A. Skardal, “Optimization of collagen type I-hyaluronan hybrid bioink for 3D bioprinted liver microenvironments,” *Biofabrication*, vol. 11, no. 1, pp. 11–14, 2019, doi: 10.1088/1758-5090/aae543.
- [38] Y. J. Choi *et al.*, “A 3D cell printed muscle construct with tissue-derived bioink for the treatment of volumetric muscle loss,” *Biomaterials*, vol. 206, no. March, pp. 160–169, 2019, doi: 10.1016/j.biomaterials.2019.03.036.

- [39] S. V. Murphy, A. Skardal, and A. Atala, "Evaluation of hydrogels for bio-printing applications," *J. Biomed. Mater. Res. - Part A*, vol. 101 A, no. 1, pp. 272–284, 2013, doi: 10.1002/jbm.a.34326.
- [40] V. Chan, P. Zorlutuna, J. H. Jeong, H. Kong, and R. Bashir, "Three-dimensional photopatterning of hydrogels using stereolithography for long-term cell encapsulation," *Lab Chip*, vol. 10, no. 16, pp. 2062–2070, 2010, doi: 10.1039/c004285d.
- [41] A. S. Hoffman, "Hydrogels for biomedical applications," *Adv. Drug Deliv. Rev.*, vol. 64, no. SUPPL., pp. 18–23, 2012, doi: 10.1016/j.addr.2012.09.010.
- [42] P. S. Gungor-Ozkerim, I. Inci, Y. S. Zhang, A. Khademhosseini, and M. R. Dokmeci, "Bioinks for 3D bioprinting: An overview," *Biomater. Sci.*, vol. 6, no. 5, pp. 915–946, 2018, doi: 10.1039/c7bm00765e.
- [43] S. G. Chen *et al.*, *Vascular Tissue Engineering: Advanced Techniques and Gene Editing in Stem Cells for Graft Generation*, vol. 27, no. 1. 2021.
- [44] B. Duan, L. A. Hockaday, K. H. Kang, and J. T. Butcher, "3D Bioprinting of heterogeneous aortic valve conduits with alginate/gelatin hydrogels," *J. Biomed. Mater. Res. - Part A*, vol. 101 A, no. 5, pp. 1255–1264, 2013, doi: 10.1002/jbm.a.34420.
- [45] B. Duan, L. A. Hockaday, K. H. Kang, and J. T. Butcher, "3D Bioprinting of heterogeneous aortic valve conduits with alginate/gelatin hydrogels," *J. Biomed. Mater. Res. - Part A*, vol. 101 A, no. 5, pp. 1255–1264, 2013, doi: 10.1002/jbm.a.34420.
- [46] Y. Wu, L. Heikal, G. Ferns, P. Ghezzi, A. Nokhodchi, and M. Maniruzzaman, "3D bioprinting of novel biocompatible scaffolds for endothelial cell repair," *Polymers (Basel)*, vol. 11, no. 12, pp. 1–12, 2019, doi: 10.3390/polym11121924.

- [47] W. W. Chan, D. C. L. Yeo, V. Tan, S. Singh, D. Choudhury, and M. W. Naing, "Additive biomanufacturing with collagen inks," *Bioengineering*, vol. 7, no. 3, pp. 1–23, 2020, doi: 10.3390/bioengineering7030066.
- [48] N. Siddiqui, S. Asawa, B. Birru, R. Baadhe, and S. Rao, "PCL-Based Composite Scaffold Matrices for Tissue Engineering Applications," *Mol. Biotechnol.*, vol. 60, no. 7, pp. 506–532, 2018, doi: 10.1007/s12033-018-0084-5.
- [49] B. Azimi, P. Nourpanah, M. Rabiee, and S. Arbab, "Poly (ϵ -caprolactone) fiber: An overview," *J. Eng. Fiber. Fabr.*, vol. 9, no. 3, pp. 74–90, 2014, doi: 10.1177/155892501400900309.
- [50] S. A. Irvine and S. S. Venkatraman, "Bioprinting and differentiation of stem cells," *Molecules*, vol. 21, no. 9, 2016, doi: 10.3390/molecules21091188.
- [51] A. Uccelli, L. Moretta, and V. Pistoia, "Mesenchymal stem cells in health and disease," *Nat. Rev. Immunol.*, vol. 8, no. 9, pp. 726–736, 2008, doi: 10.1038/nri2395.
- [52] J. J. Minguell, A. Erices, and P. Conget, "Mini-Review: Mesenchymal Cells," *Stem Cell Technol.*, vol. 226, no. June, pp. 1–5, 2001, [Online]. Available: <http://journals.sagepub.com/doi/10.1177/153537020122600603>.
- [53] L. Chen-Konak, A. Fine, and S. Levenberg, "Embryonic stem cells," *Stem Cells Revascularization Ther.*, vol. 1998, pp. 3–30, 2011, doi: 10.2165/00124363-200620020-00004.
- [54] M. C. O. Englund, P. Sartipy, and J. Hyllner, "Human embryonic stem cells," *Regen. Med. From Protoc. to Patient*, vol. 10, pp. 169–186, 2011, doi: 10.1007/978-90-481-9075-1_7.

- [55] R. Sharma, I. P. M. Smits, L. De La Vega, C. Lee, and S. M. Willerth, “3D Bioprinting Pluripotent Stem Cell Derived Neural Tissues Using a Novel Fibrin Bioink Containing Drug Releasing Microspheres,” *Front. Bioeng. Biotechnol.*, vol. 8, no. February, pp. 1–12, 2020, doi: 10.3389/fbioe.2020.00057.

List of Appendices

Appendix 1

List of Figures

1. *Figure.1.1. Factors affecting printability*
2. *Figure 1.2. Current bioprinting technologies and their subdivisions.*
3. *Figure. 1.3. The two-dimensional patterning of PLGA onto the culture substrates.*
(I) Optical micrographs of inkjet-printed PLGA patterns. The inserts represent the patterns designed using Adobe Photoshop CS software. (a) Surface profile of line pattern, (b) microscopic images of various patterns. Scale bars represent 500 mm. (II) Fluorescence microscope images of HASCs on PLGA-patterned PS substrates after 5 days of culture. (a and b) Dot pattern, (c and d) brick pattern, (e and f) "CELL" letter pattern, and (g and h) flower pattern. White bars represent 500 mm.
4. *Figure.1.4. Laser-based bioprinting: (a) A schematic of laser-based bioprinting (LDW and LAB), (b) Different cell types printed in close contact to each other with a high cell concentration, (c) Chondrocytes stained with Calcein, and (d) Osteoblast cells stained with Dil-LDL Journal*
5. *Figure .1.5.Schematic of Stereolithography Bioprinting. Photopolymerization occurs on the surface of the vat where the light-sensitive bioink is exposed to light energy. Axial platform moves downward the Z-axis during fabrication. This layer-by-layer technique does not depend on the complexity of the design, rather on its height*
6. *Figure.1.6. (a) Schematic illustration of the decellularized extracellular matrix (dECM) bioink preparation, muscle construct fabrication, and volumetric muscle loss (VML) treatment. (b) Design of muscle construct. (c) 3D cell printing of muscle construct using a granule-based reservoir system. (d) 3D cell printed muscle construct.*
7. *Figure.1.7. The structural forms of collagen and their native interactions. The basic collagen unit is a triple-helix microfibril that denatures into gelatine or can be assembled into collagen fibrils. Decorin proteins wrap around collagen fibrils in their native context and bind with glycosaminoglycan chains such as dermatan sulphate.*

8. *Figure.1.8. Polymerization of PCL by the opening of the cyclic form in the presence of heat as a catalyst*
9. *Figure. 2.1. First design in Shapr3D for the CELLINK+ bioprinter*
10. *Figure.2.2. Fixture design 1 Version 1 (B1V1)*
11. *Figure.2.3. Fixture Design 2 Version 1 (B2V1)*
12. *Figure.2.4. Bed profiles and printer settings*
13. *Figure.2.5. Filament settings and fan settings.*
14. *Figure. 2.6. Visualization of the travel path and retractions*
15. *Figure. 2.7. Skirt and Brim.*
16. *Figure. 2.8. Layers and perimeters settings*
17. *Figure.2.9. Infill settings*
18. *Figure. 2.10. Concentric print with infill first mode*
19. *Figure.2.11. Platter containing all the print constructs*
20. *Figure.2.12. changes made during optimization of software.*
21. *Figure.2.13. Verification of B2V1 fixture design*
22. *Figure.2.14. The printed construct on nanofiber substrate submerged in culture medium.*
23. *Figure.2.15. Images showing nuclei of porcine stem cells, taken from a fluorescence microscope (a) Print1 (b) Print2.*
24. *Figure.2.17. The algorithm implemented for cell detection*
25. *Figure.3.1. Picture of B2V1 fixture machined*
26. *Figure.3.2. They are the constructs printed while optimizing the python code for the bioprinter*
27. *Figure.3.3. Print1 : (A) Original RGB image, (B) Red channel isolated and contrast adjusted, (C) Edge detection using “Canny” filter, (D) Holed filled and the image cleaned for measurements.*
28. *Figure.3.4. Print2 : (A) Original RGB image, (B) Red channel isolated and contrast adjusted, (C) Edge detection using “Canny” filter, (D) Holed filled and the image cleaned for measurements.*

29. *Figure.3.5.(A) Centroids mapped on the Grayscale images of Print1 and (B)Centroids mapped on the Grayscale images of Print2.*
30. *Figure.4.1. (A)The output of Image through Canny method, (B)Output of Image through Prewitt method, (C)Output of Image through Roberts method, (D)Output of Image through LoG method,(E)Output of Image through Approxanny method, (F) The mean image of all the method outputs and set all values higher than 0 to 1.*
31. *Figure.4.2. Magnified and contrast-enhanced images of bubble artifacts in the printed construct*

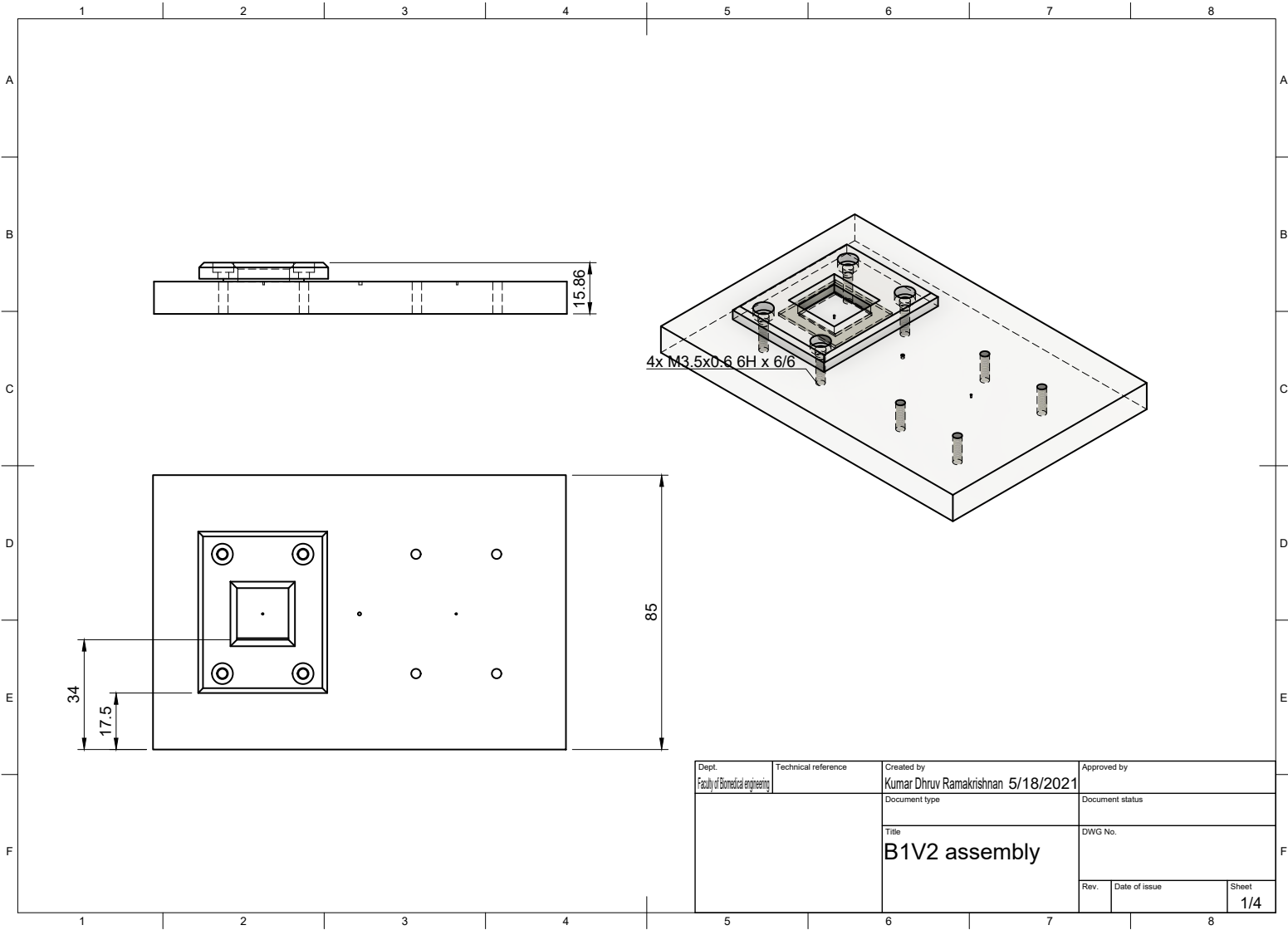
Appendix 2

List of Tables

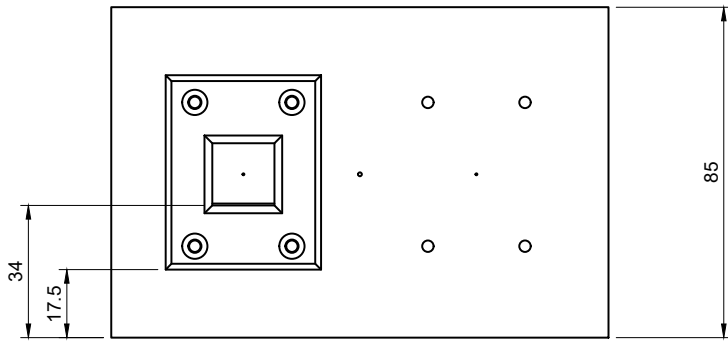
1. *Table. 2.1. Dimensions of constructs to be printed*
2. *Table 3.1 Results of the verification process.*
3. *Table.3.2. Results from the processing code for Print1*
4. *Table.3.3. Results from the processing code for Print2*

Appendix 3

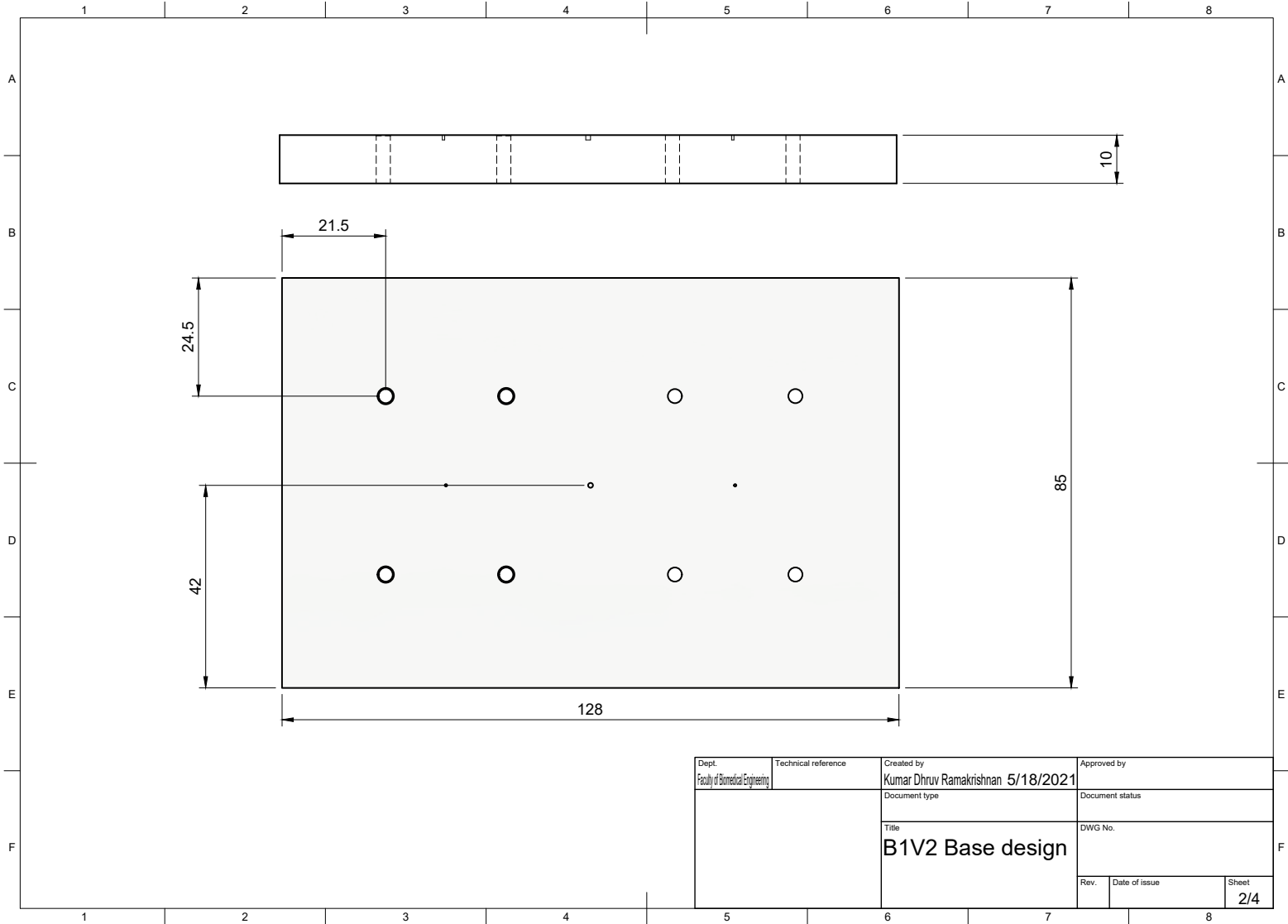
Engineering drawings of the developed fixtures



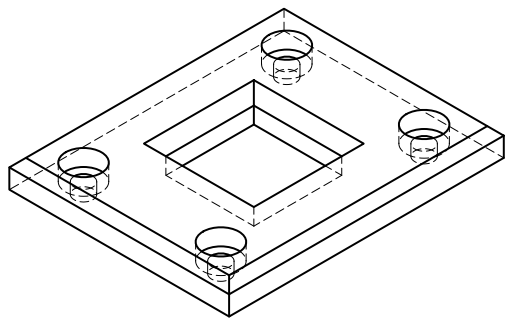
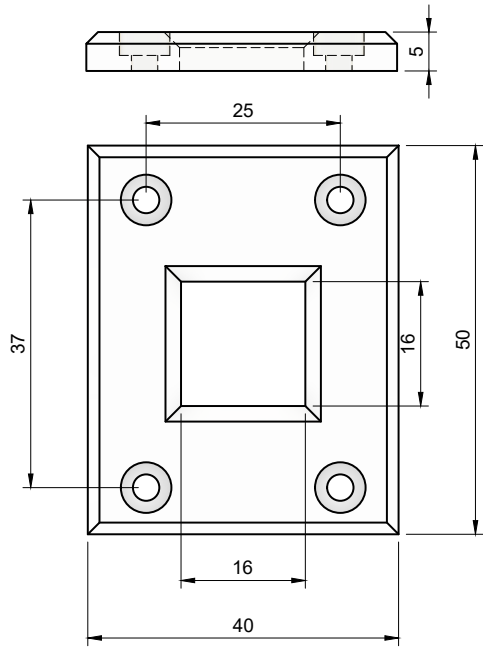
4x M3.5x0.6H x 6/6



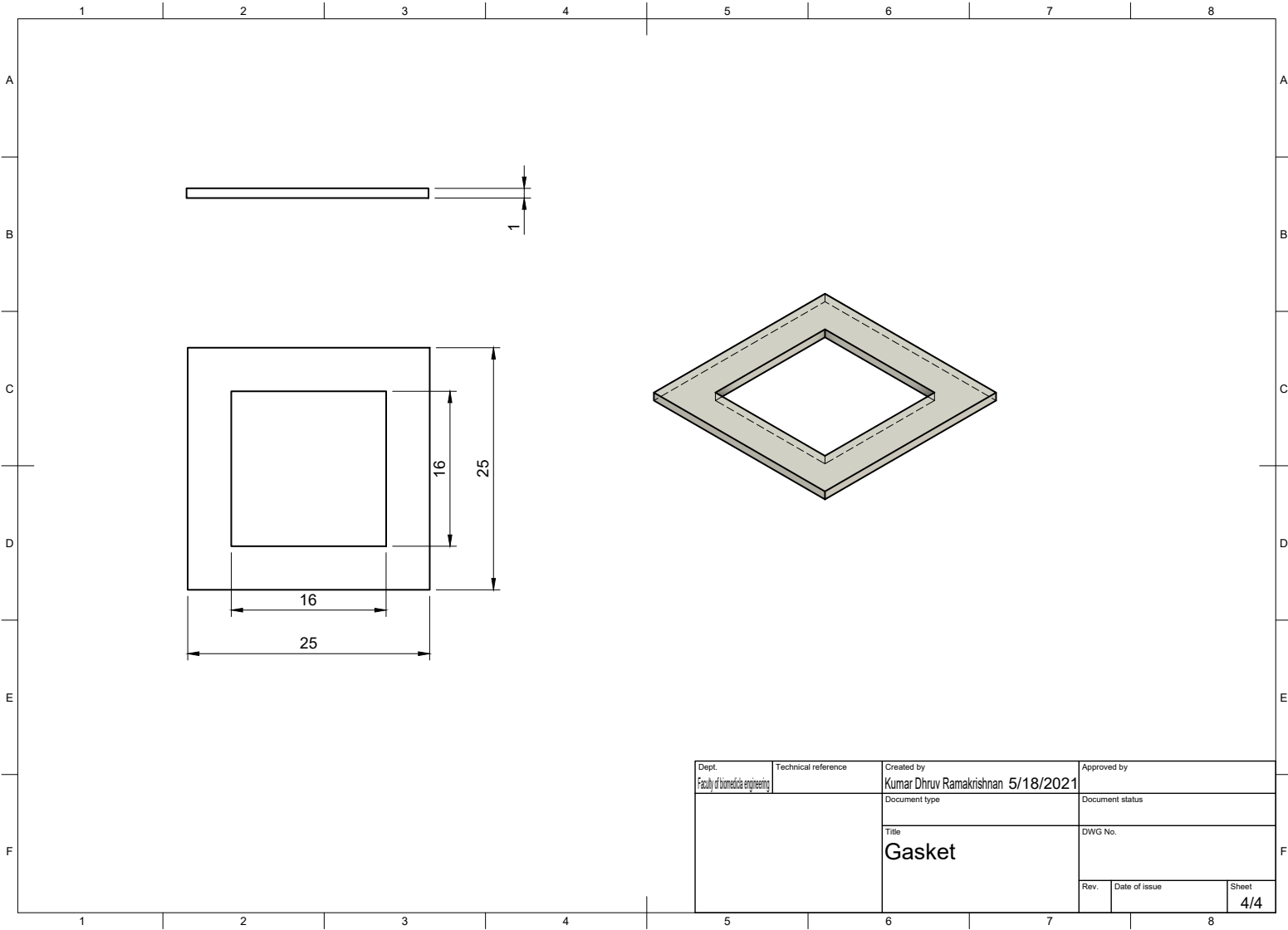
Dept. Faculty of Biomedical engineering	Technical reference	Created by Kumar Dhruv Ramakrishnan 5/18/2021	Approved by	
		Document type	Document status	
		Title B1V2 assembly	DWG No.	
		Rev.	Date of issue	Sheet 1/4



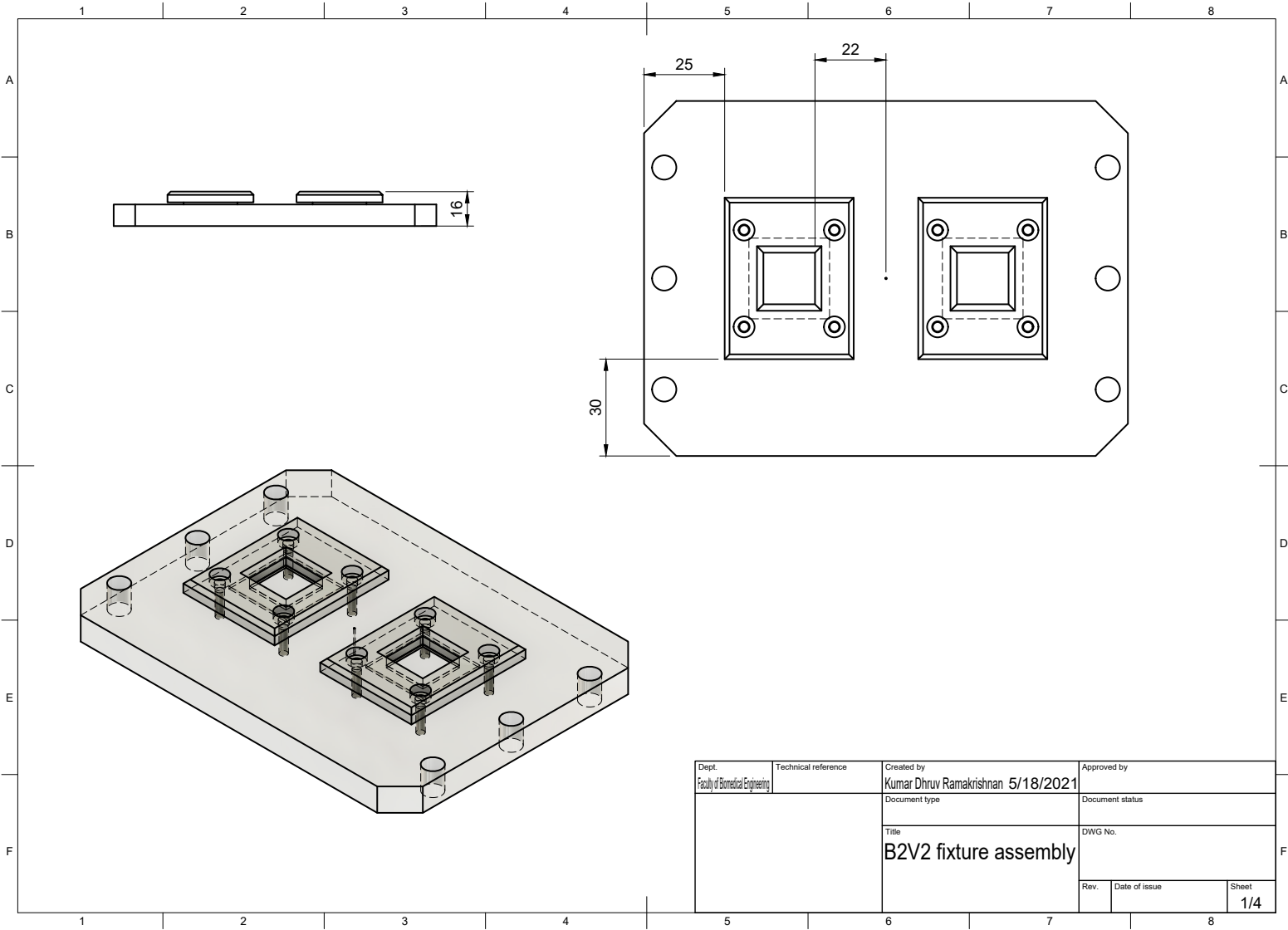
Dept. Faculty of Biomedical Engineering	Technical reference	Created by Kumar Dhruv Ramakrishnan 5/18/2021	Approved by
		Document type	Document status
		Title B1V2 Base design	DWG No.
		Rev.	Date of issue
			Sheet 2/4



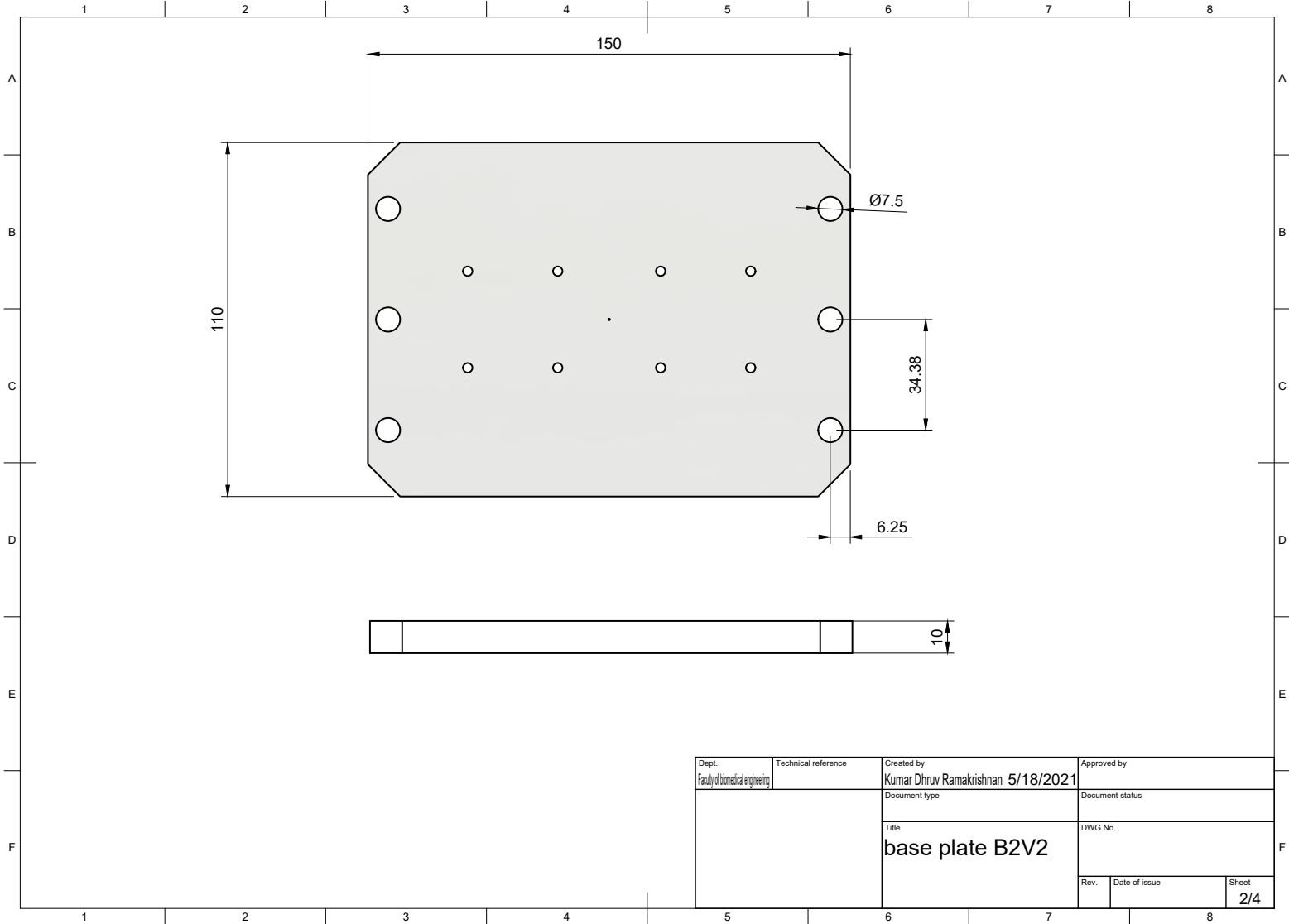
Dept. Faculty of Biomedical Engineering	Technical reference	Created by Kumar Dhruv Ramakrishnan 5/18/2021	Approved by
		Document type	Document status
		Title Clip design	DWG No.
		Rev.	Date of issue
			Sheet 3/4



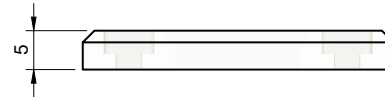
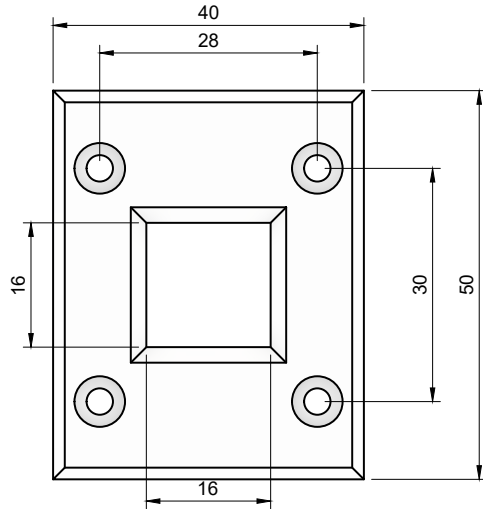
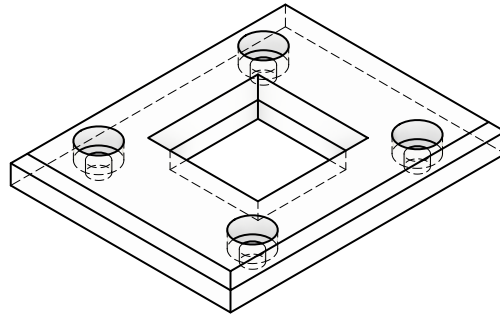
Dept. Faculty of biomedical engineering	Technical reference	Created by Kumar Dhruv Ramakrishnan 5/18/2021	Approved by
		Document type	Document status
		Title Gasket	DWG No.
		Rev.	Date of issue
			Sheet 4/4



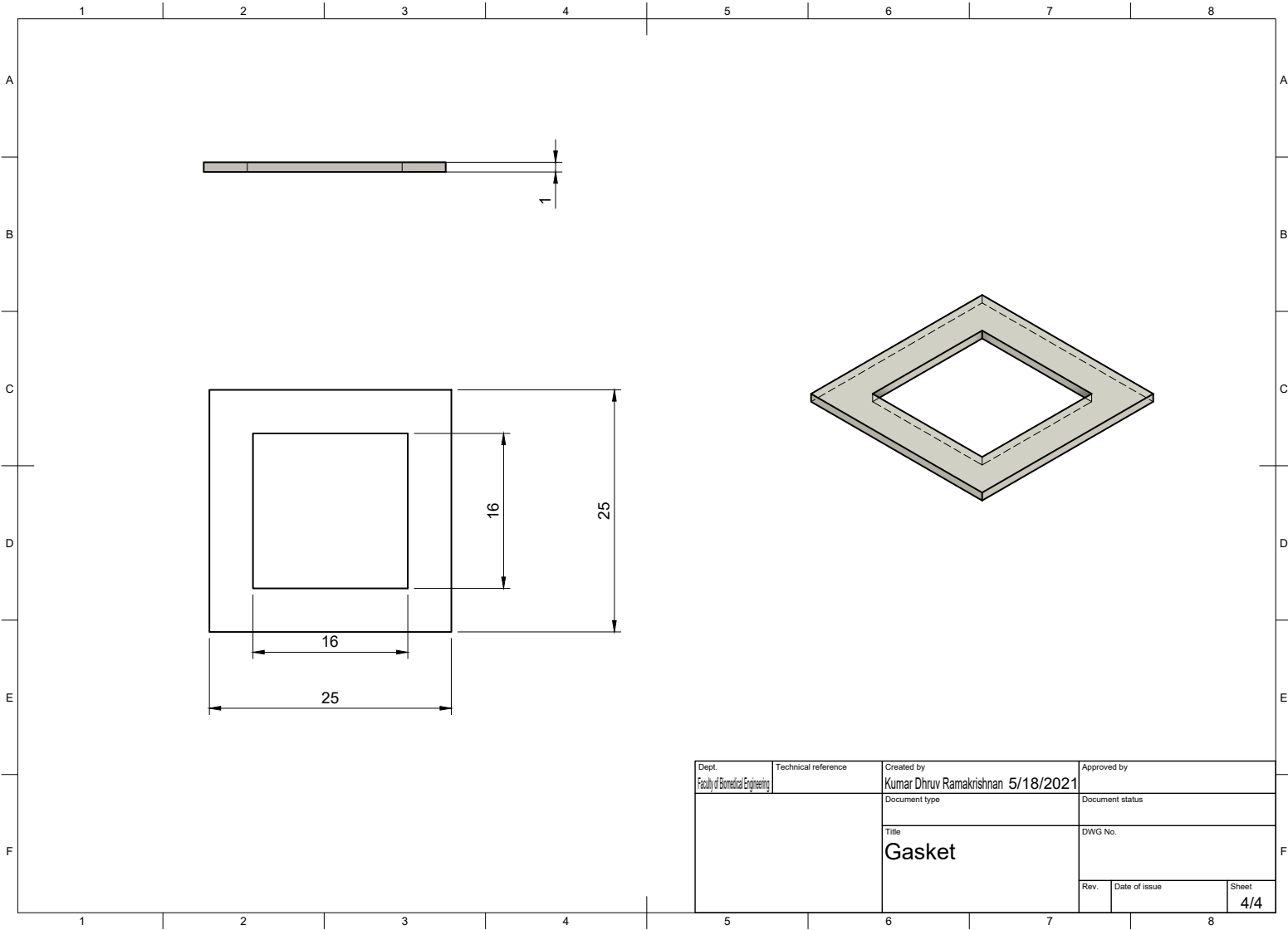
Dept. Faculty of Biomedical Engineering	Technical reference	Created by Kumar Dhruv Ramakrishnan 5/18/2021	Approved by		
		Document type	Document status		
		Title B2V2 fixture assembly	DWG No.		
		Rev.	Date of issue	Sheet 1/4	



Dept. Faculty of biomedical engineering	Technical reference	Created by Kumar Dhruv Ramakrishnan 5/18/2021	Approved by
		Document type	Document status
		Title base plate B2V2	DWG No.
		Rev.	Date of issue
			Sheet 2/4



Dept. Faculty of biomedical engineering	Technical reference	Created by Kumar Dhruv Ramakrishnan 5/18/2021	Approved by
		Document type	Document status
		Title Clip design	DWG No.
		Rev.	Date of issue
			Sheet 3/4



Dept. Faculty of Biomedical Engineering	Technical reference	Created by Kumar Dhruv Ramakrishnan 5/18/2021	Approved by	
		Document type	Document status	
		Title Gasket	DWG No.	
		Rev.	Date of issue	Sheet 4/4